



**UNIVERSIDAD DE INVESTIGACIÓN DE  
TECNOLOGÍA EXPERIMENTAL  
YACHAY**

Escuela de Ciencias Biológicas e Ingeniería

**TÍTULO:**

Biomechanical analysis of idiopathic osteodegenerative scoliosis of the lumbar spine through finite element analysis

Trabajo de integración curricular presentado como  
requisito para la obtención  
del título de Ingeniería Biomédica

**Autor:**

Obando Angulo Gabriela Belén

**Tutor:**

Mgs. Villalba Meneses, Gandhi Fernando

Urcuquí, enero 2022

**SECRETARÍA GENERAL**  
**(Vicerrectorado Académico/Cancillería)**  
**ESCUELA DE CIENCIAS BIOLÓGICAS E INGENIERÍA**  
**CARRERA DE BIOMEDICINA**  
**ACTA DE DEFENSA No. UITEY-BIO-2022-00003-AD**

A los 11 días del mes de enero de 2022, a las 11:30 horas, de manera virtual mediante videoconferencia, y ante el Tribunal Calificador, integrado por los docentes:

<b>Presidente Tribunal de Defensa</b>	Dr. GUDIÑO GOMEZJURADO, MARCO ESTEBAN , Ph.D.
<b>Miembro No Tutor</b>	Dr. ALMEIDA GALARRAGA, DIEGO ALFONSO , Ph.D.
<b>Tutor</b>	Mgs. VILLALBA MENESES, GANDHI FERNANDO

El(la) señor(ita) estudiante **OBANDO ANGULO, GABRIELA BELEN**, con cédula de identidad No. **1725210841**, de la **ESCUELA DE CIENCIAS BIOLÓGICAS E INGENIERÍA**, de la Carrera de **BIOMEDICINA**, aprobada por el Consejo de Educación Superior (CES), mediante Resolución **RPC-SO-43-No.496-2014**, realiza a través de videoconferencia, la sustentación de su trabajo de titulación denominado: **Biomechanical analysis of idiopathic osteodegenerative scoliosis of the lumbar spine through finite element análisis**, previa a la obtención del título de **INGENIERO/A BIOMÉDICO/A**.

El citado trabajo de titulación, fue debidamente aprobado por el(los) docente(s):

<b>Tutor</b>	Mgs. VILLALBA MENESES, GANDHI FERNANDO
--------------	--

Y recibió las observaciones de los otros miembros del Tribunal Calificador, las mismas que han sido incorporadas por el(la) estudiante.

Previamente cumplidos los requisitos legales y reglamentarios, el trabajo de titulación fue sustentado por el(la) estudiante y examinado por los miembros del Tribunal Calificador. Escuchada la sustentación del trabajo de titulación a través de videoconferencia, que integró la exposición de el(la) estudiante sobre el contenido de la misma y las preguntas formuladas por los miembros del Tribunal, se califica la sustentación del trabajo de titulación con las siguientes calificaciones:

Tipo	Docente	Calificación
Tutor	Mgs. VILLALBA MENESES, GANDHI FERNANDO	10,0
Presidente Tribunal De Defensa	Dr. GUDIÑO GOMEZJURADO, MARCO ESTEBAN , Ph.D.	10,0
Miembro Tribunal De Defensa	Dr. ALMEIDA GALARRAGA, DIEGO ALFONSO , Ph.D.	10,0

Lo que da un promedio de: **10 (Diez punto Cero)**, sobre 10 (diez), equivalente a: **APROBADO**

Para constancia de lo actuado, firman los miembros del Tribunal Calificador, el/la estudiante y el/la secretario ad-hoc.

Certifico que *en cumplimiento del Decreto Ejecutivo 1017 de 16 de marzo de 2020, la defensa de trabajo de titulación (o examen de grado modalidad teórico práctica) se realizó vía virtual, por lo que las firmas de los miembros del Tribunal de Defensa de Grado, constan en forma digital.*

OBANDO ANGULO, GABRIELA BELEN

**Estudiante** MARCO ESTEBAN GUDINO GOMEZJURADO  
 Firmado digitalmente por MARCO ESTEBAN GUDINO GOMEZJURADO  
 Fecha: 2022.01.11 15:55:16 -05'00'

Dr. GUDIÑO GOMEZJURADO, MARCO ESTEBAN , Ph.D.  
**Presidente Tribunal de Defensa**

 Firmado electrónicamente por:  
 GANDHI FERNANDO VILLALBA MENESES, GANDHI FERNANDO



Firmado electrónicamente por:

**DIEGO ALFONSO  
ALMEIDA  
GALARRAGA**

Dr. ALMEIDA GALARRAGA, DIEGO ALFONSO , Ph.D.

**Miembro No Tutor**



Firmado electrónicamente por:

**KARLA  
ESTEFANIA  
ALARCON FELIX**

ALARCON FELIX, KARLA ESTEFANIA

**Secretario Ad-hoc**

**Autoría**

Yo, GABRIELA BELÉN OBANDO ANGULO, con cédula de identidad 1725210841, declaro que las ideas, juicios, valoraciones, interpretaciones, consultas bibliográficas, definiciones y conceptualizaciones expuestas en el presente trabajo; así como, los procedimientos y herramientas utilizadas en la investigación, son de absoluta responsabilidad de el/la autor (a) del trabajo de investigación curricular. Así mismo, me acojo a los reglamentos internos de la Universidad de Investigación de Tecnología Experimental Yachay.

Urququí, noviembre 2021.



Gabriela Belén Obando Angulo

CI: 1725210841

### **Autorización de publicación**

Yo, GABRIELA BELÉN OBANDO ANGULO, con cédula de identidad 1725210841, cedo a la Universidad de Investigación de Tecnología Experimental Yachay, los derechos de publicación de la presente obra, sin que deba haber un reconocimiento económico por este concepto. Declaro además que el texto del presente trabajo de titulación no podrá ser cedido a ninguna empresa editorial para su publicación u otros fines, sin contar previamente con la autorización escrita de la universidad.

Asimismo, autorizo a la universidad que realice la digitación y publicación de este trabajo de investigación curricular en el repositorio virtual, de conformidad a lo dispuesto en el Art. 144 de la Ley Orgánica de Educación Superior.

Urququí, noviembre de 2021.



Gabriela Belén Obando Angulo

CI: 1725210841

### **Acknowledgements**

I thank God, for having given me all the opportunities that I have had and capacities to be able to get to where I am.

I thank my parents for all their efforts made to support me in my studies and for motivating me to continue improving myself.

To all who have been my teachers at Yachay Tech, highly trained professionals from whom I learned a lot and always showed their human side with their students. To my thesis tutor, Professor Fernando Villalba, for his always willingness to help, his patience, motivations, and all the time dedicated so that I can fulfill my degree project. To all my friends from the university, who were like a family for me during the time I lived in Yachay.

### **Dedication**

I want to dedicate this thesis and not only that but all the effort, work, and dedication behind these five years of my university career. To God for always being a pillar in my life, to my family, of course, my parents and siblings who without them I would not have reached so high, to my friends who cheered and filled my life with colors, and to me for always being persevering, for never give up.

"You have to be strong and brave"

“Gabriela B. Obando A.”

## Resumen

Los problemas asociados con la columna vertebral sobre todo en el área lumbar han incrementado considerablemente en los últimos años esto debido al sedentarismo y sobre todo el trabajo de oficina que miles de personas se han visto obligadas a tener por el cambio de rutina adquirido por la pandemia de Covid-19. Estos sucesos han provocado que cientos de personas sufran de patologías relacionadas a la columna vertebral, siendo las más comunes osteofitos y escoliosis, causando mucho dolor en el individuo y hasta problemas en la biomecánica del mismo. Muchos de los casos que no son tratados inmediatamente pueden llegar a agravarse con el tiempo provocando incluso que el paciente sea intervenido quirúrgicamente para dar solución a su patología. Es por esto que para dar un pronóstico temprano de la evolución de la patología a través del tiempo y proporcionar cuantitativamente los parámetros de fuerza y presión de los lugares específicos en los cuales hubo una mayor carga y mala distribución del peso corporal en el individuo, se ha desarrollado el siguiente estudio que por medio de los datos obtenidos y la simulación generada se puede establecer un modelo óptimo que pudo mejorar las estrategias quirúrgicas dependiendo el grado particular de la patología del objeto de estudio. Además, en la mayoría de casos si se realiza este análisis en un diagnóstico temprano se puede evitar el desarrollo de la patología y que ésta aumente a tal grado de que sea necesario una intervención quirúrgica. Es por esto que el estudio es de suma importancia médica cuyo objetivo principal es contribuir con un modelo pre-clínico para conocimiento de mejora prequirúrgica o incluso como coadyuvante en los métodos de rehabilitación puesto que a través de la simulación se conoce certeramente el lugar específico de daño espinal. Para esto se utilizó como metodología el análisis de

elementos finitos que a través de los softwares mimics materialize, ansys (icem), gvin y abaqus se pudo obtener un modelo muy fiable para el análisis de la patología del individuo. Finalmente, con ayuda del modelo se pudo determinar los puntos específicos de presión así como dar un diagnóstico certero para mejorar la patología dando como resultado una inminente intervención quirúrgica debido a las agravaciones patológicas del individuo. Por lo cual se puede concluir que la simulación obtenida por análisis de elementos finitos es un método simple, práctico y económico además de la predicción de daños en áreas específicas del cuerpo humano así como parámetros definidos para reducir el daño al cuerpo humano. columna vertebral. mejorando los hábitos. Además, es un gran aliado en los estudios médicos porque aporta una amplia variedad de datos sobre la composición y comportamiento de tejidos o áreas de estudio específico.

**Palabras clave:** escoliosis, análisis de elementos finitos, vértebras, osteofitos, calcificación de disco.

## **Abstract**

The problems associated with the spine, especially in the lumbar area, have increased considerably in recent years, due to sedentary lifestyles and especially the office work that thousands of people have been forced to have due to the change in routine acquired by the pandemic of Covid-19. These events have caused hundreds of people to suffer from pathologies related to the spine, the most common being osteophytes and scoliosis, causing a lot of pain in the individual and even problems in the biomechanics of the patient. Many of the cases that are not treated immediately can get worse over time, even causing the patient to undergo surgery to solve their pathology. This is why to give an early prognosis of the evolution of the pathology over time and quantitatively provide the force and pressure parameters of the specific places in which there is a greater load and poor distribution of body weight in the individual, has developed the following study that using the data obtained and the simulation generated, an optimal model can be established to improve surgical strategies depending on the particular degree of the individual's pathology. In addition, in most cases, if this analysis is performed in an early diagnosis, the development of the pathology can be avoided, and that it increases to such a degree that surgical intervention is necessary. This is why the study is of great medical importance, the main objective of which is to contribute with a pre-clinical model for knowledge of pre-surgical improvement or even as an adjunct in rehabilitation methods since through simulation the specific place of the spinal damage. For this, the finite element analysis was used as a methodology that through the software mimics materialize, ansys (icem), gwin and abaqus it was possible to obtain a very reliable

model for the analysis of the individual's pathology. Finally, with the help of the model, it was possible to determine the specific pressure points as well as to give an accurate diagnosis to improve the pathology, resulting in an imminent surgical intervention due to the pathological aggravations of the individual. Therefore, it can be concluded that the simulation obtained by finite element analysis is a simple, practical and economical method in addition to the prediction of damage in specific areas of the human body as well as defined parameters to reduce damage to the human body. spine. improving habits. In addition, it is a great ally in medical studies because it provides a wide variety of data on the composition and behavior of tissues or specific areas of study.

**Keywords:** scoliosis, finite element analysis, vertebrae, osteophytes, disc calcification.

**Table of Contents**

<b>1. Objectives.....</b>	<b>20</b>
1.1. General objective.....	20
1.2. Specific objectives.....	20
<b>2. Scope of the study.....</b>	<b>21</b>
<b>3. Background.....</b>	<b>22</b>
<b>4. General Introduction to Scoliosis.....</b>	<b>23</b>
4.1. Front view classification.....	24
4.1.1. Classification according to the type of scoliosis.....	24
4.1.2. Classification according to the origin of scoliosis.....	25
4.1.3. Idiopathic scoliosis.....	26
4.1.3.1. Cobb angle.....	27
4.1.3.2. Ferguson's method.....	29
4.2. Cross-sectional view classification.....	30
4.2.1. Lordosis.....	30
4.2.1.1. Sagittal arrows test.....	31
4.2.1.2. Lordosis angle measurement.....	32
4.3. Calcification of intervertebral discs.....	34
4.4. Osteophytes.....	35
4.4.1. Marginal osteophytes.....	35
4.4.2. Central osteophytes.....	36

4.5.	Bone.....	37
4.5.1.	Cortical bone tissue.....	37
4.5.2.	Spongy bone tissue.....	38
4.6.	Intervertebral disc.....	38
5.	<b>Problem statement.....</b>	<b>40</b>
6.	<b>Methodology.....</b>	<b>41</b>
6.1.	Design and implementation of the model in mimics materialize.....	42
6.1.1.	Creation of the 3D model with mimics materialize.....	44
6.2.	Mesh design Ansys (Icem).....	48
6.3.	Finite element analysis in Abaqus.....	51
6.3.1.	Sets Creation.....	51
6.3.2.	Creation of the material.....	52
6.3.2.1.	Young's modulus and elasticity.....	52
6.3.3.	Creation of sections.....	54
6.3.4.	Seccion Assignment.....	54
6.3.5.	Loads.....	55
6.3.6.	Simulation.....	56
6.3.7.	Interface and mechanisms.....	57
7.	<b>Results.....</b>	<b>59</b>
8.	<b>Discussion.....</b>	<b>67</b>
9.	<b>Conclusion.....</b>	<b>72</b>
10.	<b>Recommendations and limitations.....</b>	<b>74</b>

<b>11. Future works.....</b>	<b>75</b>
<b>12. References.....</b>	<b>76</b>
<b>13. Annexes.....</b>	<b>84</b>

### **Index of acronyms**

**SRS:** Scoliosis Research Society.

**AIS:** Idiopathic scoliosis classification system according to the degree of scoliosis.

**Vertebra L:** corresponds to the lumbar vertebrae and is generally accompanied by a number that indicates the position of the vertebra.

**Vertebra S:** corresponds to the sacral vertebrae and is generally accompanied by a number that indicates the position of the vertebra.

**Vertebra T:** corresponds to the thoracic vertebra and is generally accompanied by a number that indicates the position of the vertebra.

**DICOM:** Digital Imaging and Communications in Medicine.

**HU:** Heat Units.

**STL:** Standard Triangle Language format to create a 3d model.

**FEM:** Finite element method.

**FSU:** Functional spinal units.

**FEA:** Finite elements analysis

**List of tables**

**Table 1.** Classification according to the type of scoliosis. Own elaboration.....24

**Table 2.** Scoliosis degrees using the Cobb method.....28

**Table 3.** HU ranges according to the area of the spine.....43

**Table 4.** Values obtained through simulation in the Ansys (Icem) program.....49

**Table 5.** Data for Finite element model of FSU.....53

**Table 6.** Von Mises maximum value in each study area.....64

**Table 7.** Displacement distance between original and deformed model.....65

### List of Figures

<b>Figure 1.</b> Classification of Kings types I, II, III, IV, and V.....	26
<b>Figure 2.</b> Measurement of scoliosis using the Cobb method.....	27
<b>Figure 3.</b> Scoliosis measurement using Fergurson's method.....	28
<b>Figure 4.</b> Classification according to the degree of curvature.....	29
<b>Figure 5.</b> Model made in Mimics materialize to determine the degree of curvature.....	30
<b>Figure 6.</b> Movement of the lumbar vertebrae causing lordosis.....	31
<b>Figure 7.</b> Measurement of lordosis according to the sagittal arrows method.....	32
<b>Figure 8.</b> Different methods for taking lordosis measurement.....	33
<b>Figure 9.</b> Measurement of lordosis according to the lordosis angle method.....	34
<b>Figure 10.</b> L2 and L3 vertebrae present disc calcification to a very high degree.....	35
<b>Figure 11.</b> Sagittal view of the lumbar spine, vertebrae T11, 12; L1,2 and 3 higher pronunciation of osteophytes.....	36
<b>Figure 12.</b> Parts of a vertebra.....	38
<b>Figure 13.</b> Editing the 3D model. Cortical area, spongy area, vertebral nucleus, fibrous rings.....	44
<b>Figure 14.</b> 3D model of intervertebral disc nucleus and fibrous rings. Figure 15. 3D model of the cancellous bone area.....	45
<b>Figure 16.</b> 3D model of the cortical bone area.....	46
<b>Figure 17.</b> 3D model of the vertebral column, last 3 dorsal vertebrae, and lumbar vertebrae.....	47

<b>Figure 18.</b> The meshing of the model in Ansys (Icem).....	<b>50</b>
<b>Figure 19.</b> Code for creating Sets in Gvim.....	<b>52</b>
<b>Figure 20.</b> Creation of the sections in Abaqus.....	<b>54</b>
<b>Figure 21.</b> Total embedment.....	<b>55</b>
<b>Figure 22.</b> Embedding interface.....	<b>56</b>
<b>Figure 23.</b> Original model. <b>Figure 24.</b> Deformed model.....	<b>59</b>
<b>Figure 25.</b> Von Mises of the cortical area.....	<b>60</b>
<b>Figure 26.</b> Von Mises close-up of the cortical area.....	<b>61</b>
<b>Figure 27.</b> Von Mises spongy area.....	<b>61</b>
<b>Figure 28.</b> Von Mises intervertebral area.....	<b>62</b>
<b>Figure 29.</b> Von Mises approaching the intervertebral area.....	<b>63</b>
<b>Figure 30.</b> Von Mises general model.....	<b>64</b>
<b>Figure 31.</b> Maximum principal stress of the generated model.....	<b>66</b>

**Schema list**

**Scheme 1.** Pathology parameters of the study subject.....37

**Scheme 2.** The general methodology for obtaining the simulation.....42

**Scheme 3.** 3D modeling general scheme.....48

**Scheme 4.** The meshing of the general scheme model.....50

**Scheme 5.** Simulation generation model in Abaqus.....57

**Scheme 6.** The general model to obtain the simulation..... 58

### **Annex index**

<b>Annex 1.</b> Coronal, axial, and sagittal view of a CT scan.....	<b>84</b>
<b>Annex 2.</b> Contrast interface.....	<b>84</b>
<b>Annex 3.</b> Interface to Edit mask, use of lasso tool to select the area.....	<b>85</b>
<b>Annex 4.</b> Interface for Boolean operation used to add or subtract .....	<b>85</b>
<b>Annex 5.</b> Interface to smooth the 3D model.....	<b>85</b>
<b>Annex 6:</b> Coronal view of the end of the dorsal vertebrae, lumbar-sacral vertebrae coccyx, floating ribs, and hip.....	<b>86</b>
<b>Annex 7.</b> Arrangement of each vertebra in the coronal plane.....	<b>86</b>
<b>Annex 8.</b> Coronal and sagittal view of the final dorsal and lumbar vertebrae.....	<b>87</b>
<b>Annex 9.</b> Add to part tool interface.....	<b>87</b>
<b>Annex 10.</b> The general meshing of the model, ribs, vertebrae, hips.....	<b>88</b>
<b>Annex 11.</b> The meshing of the sectional model of the cortical and cancellous bone area... <b>88</b>	<b>88</b>
<b>Annex 12.</b> The meshing of the model section of the area of the nucleus of the vertebra and fibrous rings.....	<b>89</b>
<b>Annex 13.</b> Moduli material of the components of FSU.....	<b>89</b>
<b>Annex 14.</b> Modeling the degeneration of aging: material moduli from healthy to fully degenerated components of FSU.....	<b>89</b>
<b>Annex 15.</b> Material creation interface in Abaqus.....	<b>90</b>
<b>Annex 16.</b> Abaqus selection creation interface.....	<b>90</b>
<b>Annex 17.</b> Abaqus assignment selection creation interface.....	<b>91</b>
<b>Annex 18.</b> Generation of Gvim code of the simulation.....	<b>93</b>

**Annex 19.** Distance between the x-plane and the greatest curvature of the original model.....**93**

**Annex 20.** Distance between the x-plane and the greatest curvature of the deformed model.....**94**

**Annex 21.** Correlation between the original and the deformed model.....**94**

**Annex 22.** Zones of Vertebral disc wedging.....**95**

**Annex 23.** Zones of Vertebral wedging..... **95**

## **1. Objectives**

### ***1.1 General Objective***

Generate a simulated model of idiopathic osteodegenerative scoliosis of the lumbar spine to provide quantitative data on the specific surfaces and points of the spine, focusing on the cortical surface, spongy and vertebral discs through Finite Element Analysis (FEA).

### ***1.2 Specific Objectives***

- Predict early damage to the spine to determine surgical need.
- Quantitatively identify the specific location of lumbar damage through Finite Element Analysis (FEA).
- Provide a reliable model of specific sites of damage as a function of time.
- Establish parameters to reduce spinal damage through improved habits.

## **2.Scope of the study**

The present study whose topic is the biomechanical analysis of idiopathic osteodegenerative scoliosis of the lumbar spine through finite element analysis. The scope of this study is based on its viability, as well as the object of study. Among the scopes it is emphasized:

1. A simulated model of the pathology of the object of study will be generated to know its biomechanics at deeper depths.
2. The efficacy of the simulation will be determined by comparing it with previous works by other authors.
3. Criteria will be established quantitatively that will serve as medical adjuvants when deciding on the treatment of the pathology.
4. An optimal model of the pathology of the object of study will be provided that can be used in several medical parameters.
5. The aim is to identify the pressure points in each research area of the project.

### 3. Background

This chapter briefly describes some of the most relevant theoretical concepts that were obtained as a basis for the realization of this project. Scoliosis has been a pathology studied for decades, however, the poor technological advances of antiquity have limited the early diagnosis and correct treatment for this disease. Additionally, one of the most used methods for the diagnosis of scoliosis was based solely on radiographs (Millner & Dickson, 1996) providing a concise diagnosis of the pathology since small details such as early osteophytes, or wedging in its initial phase were not perceived by radiographs. (Shao et al., 2002). However, in the 80s the rise of computed tomography (CT) introduced a new, much more detailed technique to know in-depth each area of the bone, so pathologies such as scoliosis were much easier to diagnose (Abul-Kasim et al., 2009).

Despite bringing great advances, the CT did not predict the pressure points or gave quantitative data of the damage in each section of the study area. That is why at the beginning of the 2000s a new method revolutionized the medical field, generating extremely reliable simulations that can predict the damage in each study area as well as provide quantitative data on pressure, temperature, etc. One of the software that revolutionized the area of structural analysis for the creation of simulations is Abaqus Finite elements analysis (FEA), which corresponds to a set of computer programs focused mainly on simulation applied to the method of finite elements to perform structural calculations. linear and non-linear static (ABAQUS Student Edition, 2021).

#### **4. General introduction of scoliosis**

The spine is the main supporting bone structure for our body, which serves in addition to supporting most of our weight, it also allows us to perform basic functions such as mobility and balance. Within this great bone structure, there are five divisions among these the cervical, dorsal, lumbar, sacral, and coxa vertebrae. All of this form a total of 33 to 34 vertebrae. (see annex 6, 7, and 8) For the present study, we will focus on the lumbar area that is composed of five lumbar vertebrae, the primary function is to support the greater weight load of our body, which is why these vertebrae are characterized by having a thicker body than the above, this is approximately 3.3 cm. In addition, this project studies the vertebral discs, which are cartilaginous structures formed by the fibrous annulus, the nucleus pulposus, and the vertebral endplates, all of which act together to stabilize the spine, serve as cushioning and distribute loads while allowing the spine to relax. flex, extend, or twist (Shao et al., 2002).

In addition, degeneration of the spine increases 8% in adults 25 years and older, and up to 68% in people 60 to 90 years (Aebi, 2005; Arlet et al., 2003). Scoliosis can be caused not only by genetic reasons but also by everyday activities such as poor posture, forced labor, among others. The severity and classification of the condition are reported according to the Cobb angle. The present investigation was carried out in an 85-year-old male patient with a clear lumbar malformation among the conditions that affect the subject, mainly scoliosis, disc calcification, and osteophyte.

##### **4.1 Front view classification**

To determine the degree of complexity of scoliosis, it must be known that it is classified in the frontal plane according to its type, degree, and origin:

### 4.1.1 Classification according to the type of scoliosis

It is divided into three types depending on the progression of the pathology and the specific area that the injury involves, we can see this in detail in Table 1.

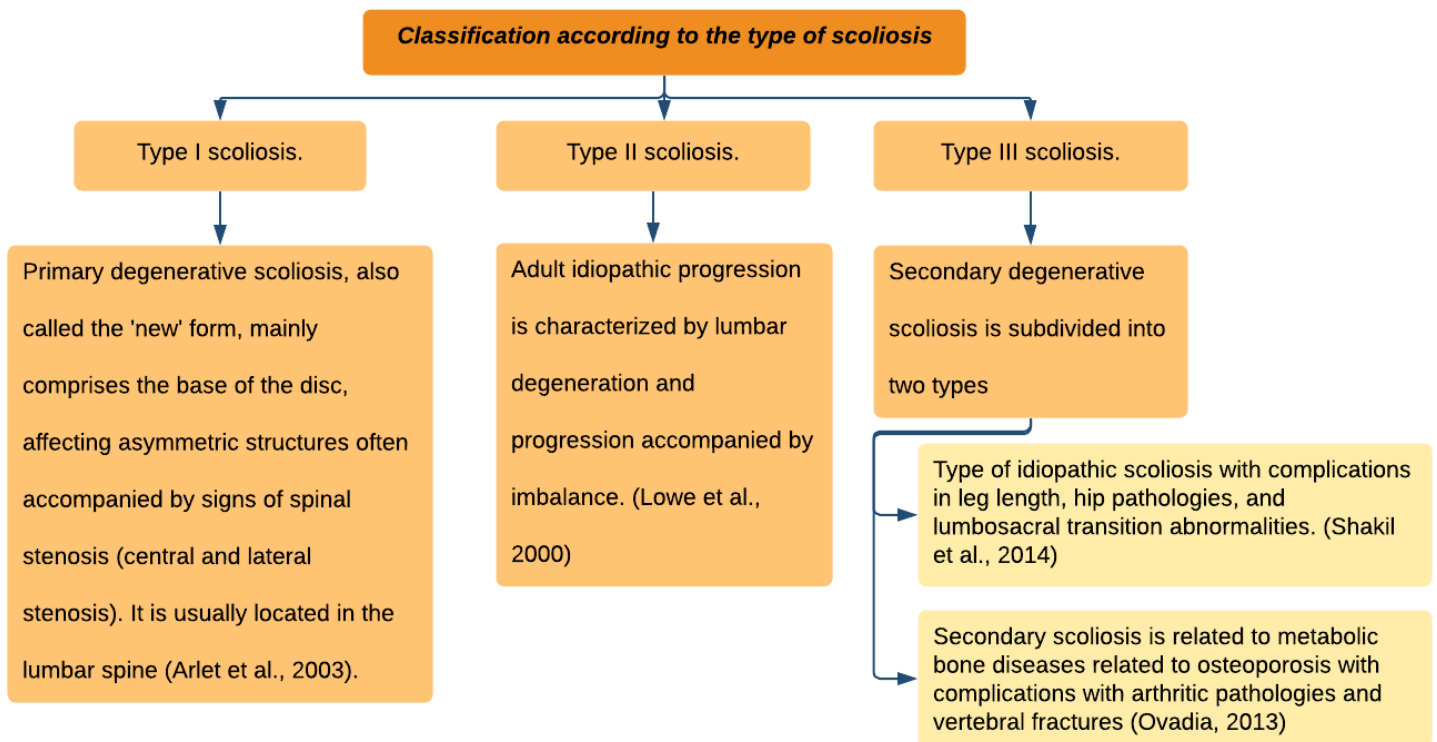


Table 1. Classification according to the type of scoliosis. Own elaboration.

#### ***4.1.1.2 Classification according to the origin of scoliosis***

Congenital scoliosis.

Genetic factors have a great influence on the development of individuals, so clinical studies indicate that in individuals with scoliosis there is a significant prevalence in people with a family history of the same type as in the general population (Arlet et al., 2003).

Neuropathic scoliosis.

The Scoliosis Research Society (SRS) classifies neuropathic scoliosis with central or peripheral motor neuron and myopathic (Rinella et al., 2004). This pathology is closely related to the disharmonious control of the trunk musculature around the spine; it is generally a progressive disorder that worsens with age, due to the lack of effective mechanisms of muscle compensation (Vialle et al., 2013).

#### ***4.1.1.3 Idiopathic scoliosis***

Beyond the classification by type or origin of scoliosis, there is its classification by the degree of complexity of the same, to determine the degree of scoliosis and its subsequent classification, the King's method is used, which determines a classification of the degree of scoliosis in 5 different degrees. This classification facilitates the objective and quantitative assessment of the disease.

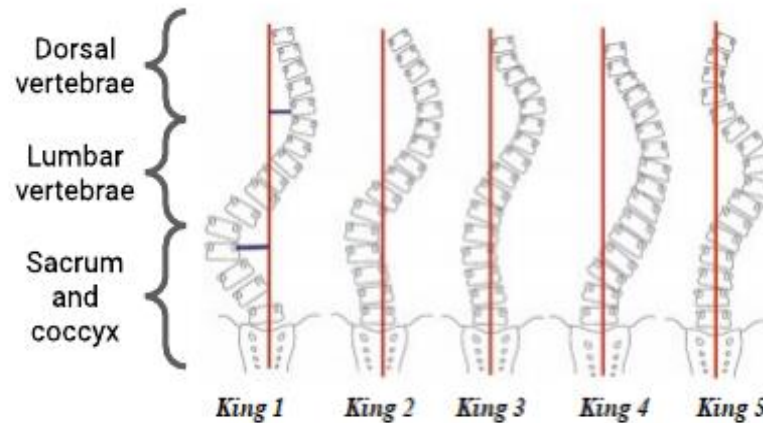


*Figure 1.* Classification of Kings types I, II, III, IV, and V. Own elaboration from [www.harms-spinesurgery.com](http://www.harms-spinesurgery.com).

In 1983 Howard King introduced the Idiopathic Scoliosis Classification System according to the degree of scoliosis called (AIS) (Richards et al., 2003). Classification according to the degree of scoliosis is based on the Cobb method.

The Ferguson and Cobb method both methods are based on the quantitative measurement of the abnormal region of the spine

#### ***4.1.3.1 Cobb angle***

The Cobb method is based on a quantitative measurement measuring the inclination of the end vertebra plate. For the Cobb method, it must be known that:

- a. Locate the initial vertebra where the abnormal deviation of the spine begins.
- b. Locate the final vertebra where the abnormal spinal deviation ends.
- c. Locate a point at the lateral end of the initial and terminal vertebrae.

Join these points with perpendicular lines. The resulting angle is the angle of the curvature (Kittleson & Lim, n.d.).

#### 4.1.3.2 Ferguson method

On the other hand, in the Ferguson method, the curvature is not affected by the inclination of the final vertebra, since performing the quantification focuses on the apex of the initial final vertebra and the mean of the abnormal curvature region of the spine. vertebral. The way to perform this method is as follows:

- a. Locate the endplate of the vertebra where the abnormal spinal deviation begins.
- b. Locate the apex of the initial, middle and final vertebrae of the deviation and mark it with a dot.
- c. Join the apex points with a perpendicular line (Diab et al., 1995).

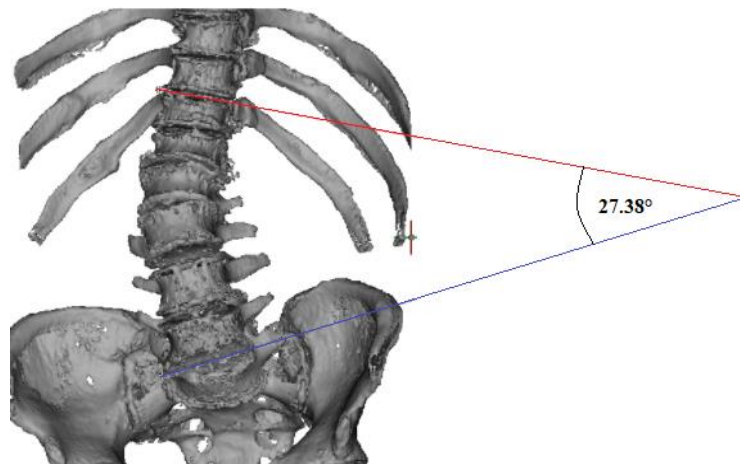
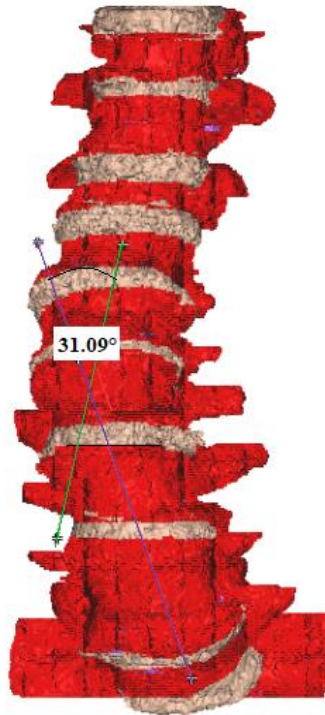


Figure 2. Measurement of scoliosis using the Cobb method. Own elaboration.



*Figure 3.* Scoliosis measurement using the Ferguson method. Own elaboration.

It should be noted that the Scoliosis Research Society has selected the Cobb measurement system as the standard system. Concluding that:

*Table 2.* Scoliosis degrees using the Cobb method. Own elaboration from Ahmadi & Salehani (2007).

<i>Grado de Escoliosis</i>	<i>Valores</i>
<i>leve</i>	10-24°
<i>moderado</i>	25-50°
<i>grave</i>	>50°

**4.1.4 Classification according to the degree of curvature**

The King's method, based on the Cobb quantification, classifies the degree of curvature of scoliosis as:

- Type I: S-shaped curvature crossing the midline of the thoracic and lumbar curves.
- Type II. the s-shaped curve in which the thoracic curve lies.
- Type III. the single thoracic curve in which no compensatory lumbar curve crosses the midline.
- Type IV: a long thoracic curve in which the fourth lumbar vertebra slopes towards the thoracic curve.
- Type V: a double thoracic curve (Richards et al., 2003).

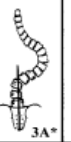
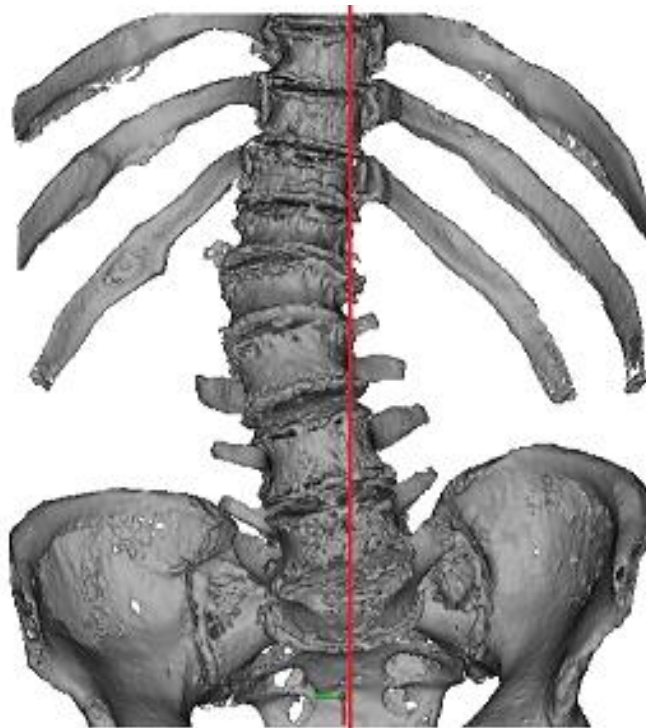
Lumbar Spine Modifier	Curve Type (1-6)					
	Type 1 (main thoracic)	Type 2 (double thoracic)	Type 3 (double major)	Type 4 (triple major)	Type 5 (TL/L)	Type 6 (TL/L- MT)
<b>A</b> (No to minimal curve)	 1A*	 2A*	 3A*	 4A*		
<b>B</b> (moderate curve)	 1B*	 2B*	 3B*	 4B*		
<b>C</b> (large curve)	 1C*	 2C*	 3C*	 4C*	 5C*	 6C*

Figure 4. Classification according to the degree of curvature. Adapted from Richards et al. (2003).



*Figure 5.* Model made in Mimics materialize to determine the degree of curvature. Own elaboration.

As can be seen in *figure 5*, the model has a 3C degree of curvature since there is a marked lumbar curve that extends to the end of the lats.

#### **4.2 Cross-sectional view classification**

Taking into account the cross-sectional view of the spine, we can name two pathologies that are lordosis and kyphosis.

##### ***4.2.1 Lordosis***

Lordosis is a condition that increases the curvature of the lower lumbar spine, or also has to do with the appearance of curvature of the posterior concavity in the dorsal region, Hyperlordosis this condition is associated with lordosis when it is above The normal ranges of curvature are characterized by the fact that a bone (vertebra) in the spinal column comes

out of the correct position on the bone that is below it and can be degenerative causing greater curvature over time as can be seen in *figure 6* (Yuing et al., 2010).

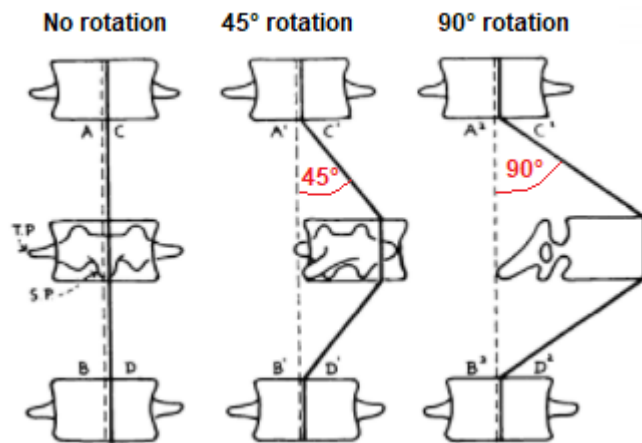


*Figure 6.* Movement of the lumbar vertebrae causing lordosis. Own elaboration from Roaf (1966).

Quantification of curvatures to correctly diagnose this pathology, it is necessary to quantify to know if the condition exists and what range it is, among the most used methods that give a very accurate calculation and do not present risk to the patient since they are methods Invasive are: sagittal arrow test and lordosis angle measurement.

#### ***4.2.1.1 Sagittal arrows test.***

It consists of evaluating the lumbar curve by determining the distance between the vertical of the plumb line, that is, the vertebra at the beginning of the curvature. To the furthest point from it, see *figure 7*. The values are classified as hyperlordosis if the value is greater than 75 °, normal between 30 and 55 °, and hyperlordosis if the value is less than 30° (Been & Kalichman, 2014).



*Figure 7.* Measurement of lordosis according to the sagittal arrows method. Own elaboration.

#### ***4.2.1.2. Lordosis angle measurement.***

This method uses different anatomical landmarks on the vertebral bodies to assess the angulation of the lordosis. Among these references can be found: tangent methods use the anterior or posterior vertebral body to determine the angle of lordosis. The centroid method uses the center of the vertebral body to measure lordosis. The best-fitting ellipse, a circular

geometric model of the lumbar spine, see *figure 8*. Furthermore, all of these methods are known to be reliable in evaluating lordosis (Been & Kalichman, 2014).

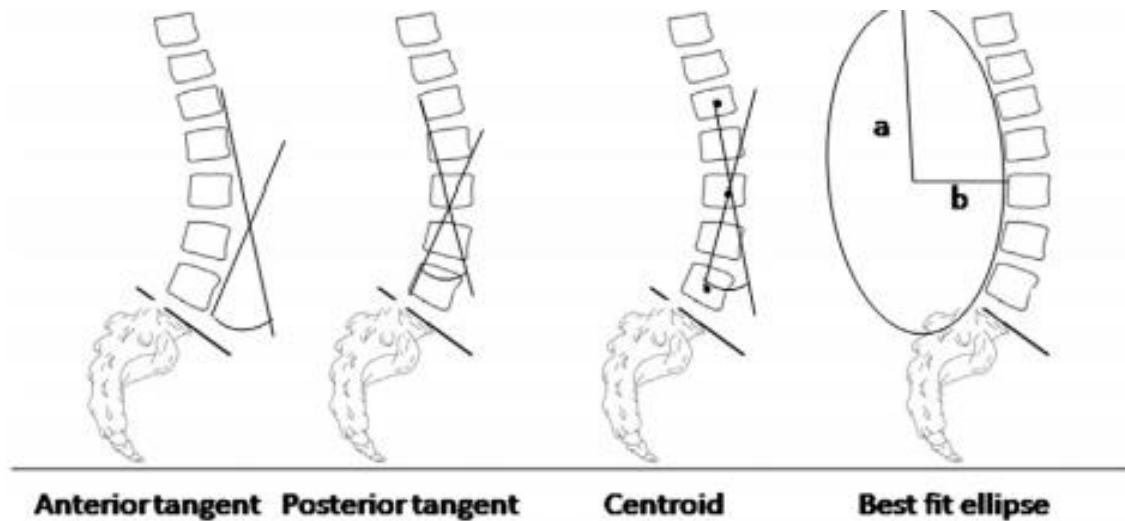


*Figure 8*. Different methods for taking lordosis measurement. Own elaboration from Been & Kalichman (2014)

In this case, to calculate the lordosis angle, we connect point T12 (thoracic vertebra 12) to point S2 (sacral vertebra 2) by a straight line, and a line perpendicular to its center is drawn passing the curve (centroid method) as it can be seen in *figure 9*. To determine the lumbar angle, the values are classified as hyperlordosis if the value is greater than  $45^\circ$ , normal between  $25^\circ$  and  $45^\circ$ , and hyperlordosis if the value is less than  $25^\circ$  (Yuing et al., 2010; Karimi et al., 2020).

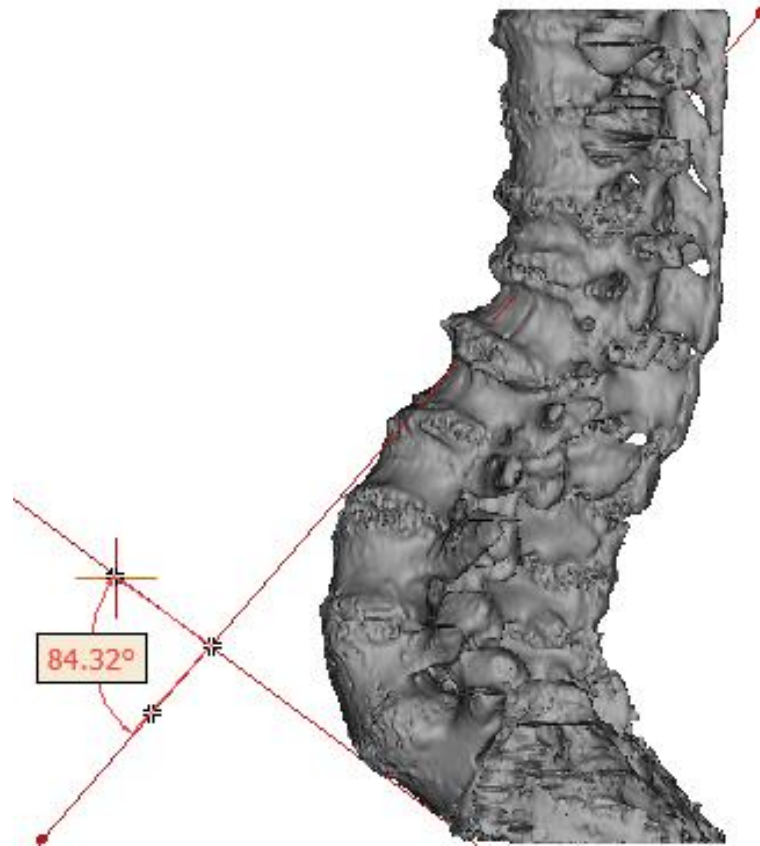
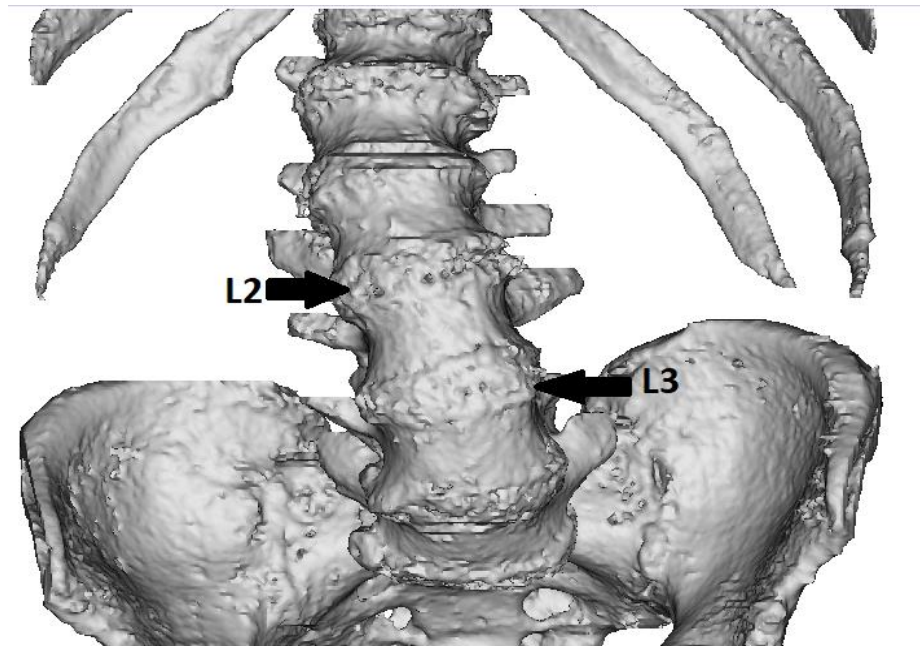


Figure 9. Measurement of lordosis according to the lordosis angle method. Own elaboration.

#### ***4.3 Calcification of intervertebral discs***

Disc calcification is a very common pathology in elderly people, generally this condition is degenerative and mainly affects the nucleus pulposus and annulus fibrosus causing a lot of pain and stiffness in movements (Gallinas et al., 2004). The 85-year-old study patient presents a serious calcification of the intervertebral discs at the level, especially in the lumbar vertebrae, as shown in *figure 10*. The vertebrae most affected are L2 and L3 in which calcification can be observed. almost complete intervertebral disc.



*Figure 10.* L2 and L3 vertebra presents disc calcification. Own elaboration.

#### ***4.4 Osteophytes***

Osteophytes are bony extensions of the periphery of the joints. In addition, they are characterized by being present in osteoarthritis of the vertebrae (Ovadia, 2006).

##### ***4.4.1 Osteofitos Marginales***

They are located on the periphery and appear in the form of an external projection in the form of a 'lip'. They are usually found in adjacent pressure segments and are predominant on one side of the joint, see *figure 11* (Arlet et al., 2003; Him et al., 2016).

#### *4.4.2 Central osteophytes*

These types of osteophytes are internal projections of the joints and have irregular rough joints. These types of osteophytes are caused by hypervascularization of the joint (Kyung et al., 2009).

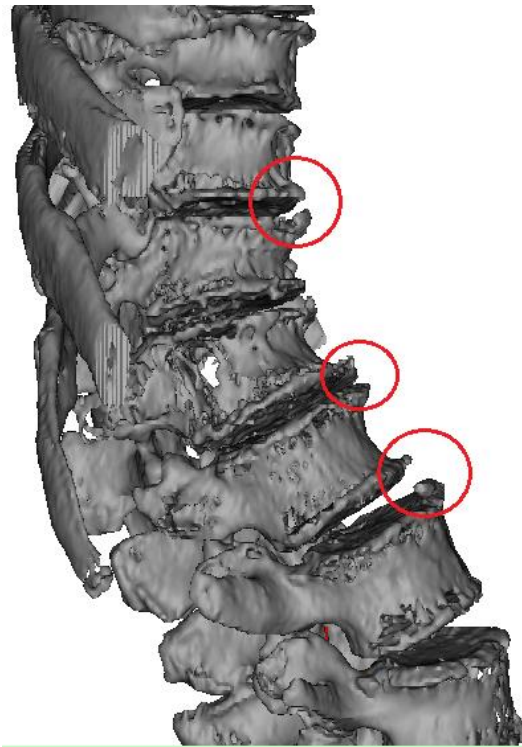
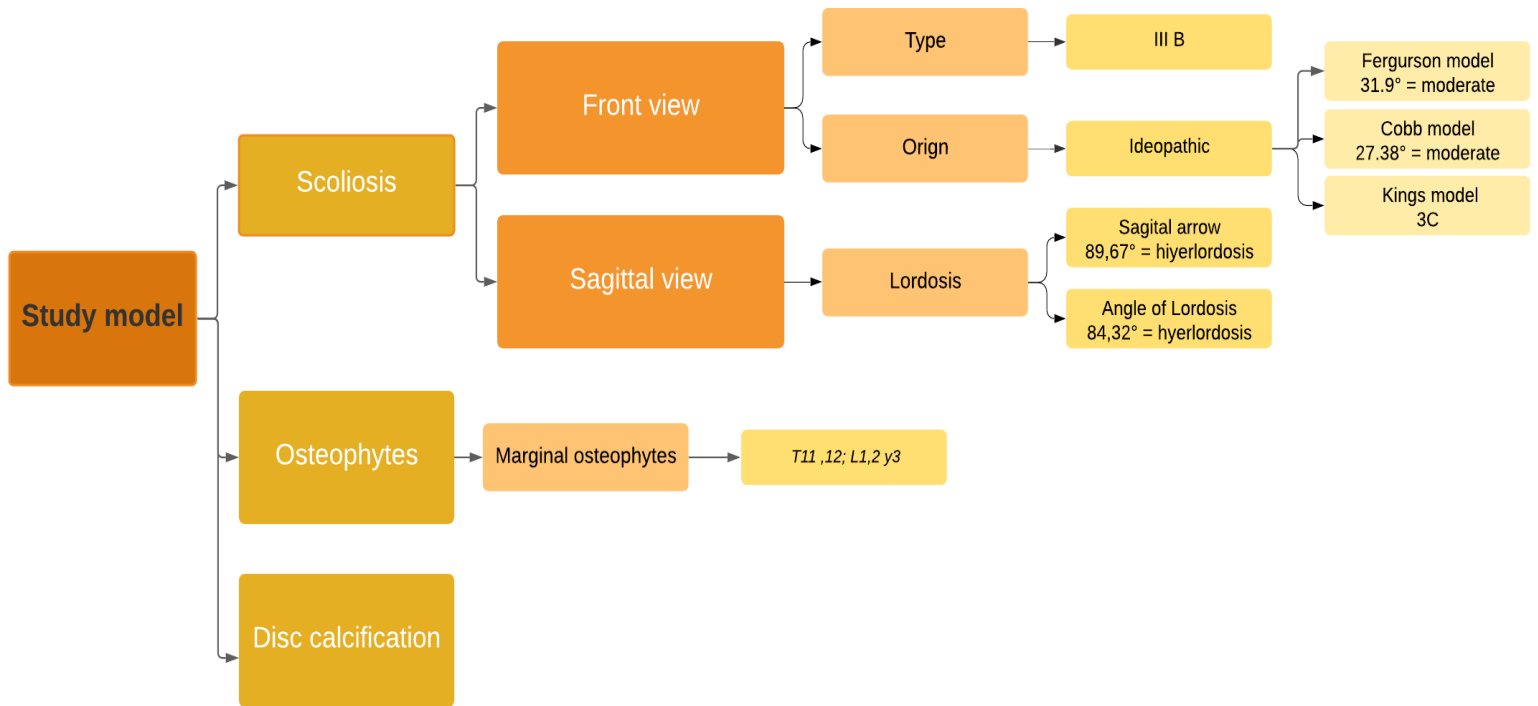


*Figure 11.* Sagittal view of the lumbar spine, vertebrae T11, 12; L1,2 and 3 higher pronunciation of osteophytes. Own elaboration.



*Scheme 1:* Pathology parameters of the study subject. Own Elaboration.

#### **4.5 Bone**

Bone tissue is a specialized connective tissue characterized by its cellular calcification and extracellular components that together form the bone matrix. This fabric is characterized by rigidity and its great resistance to pressure traction, compression. (Fawcett, D. W. 1996).

#### **4.5.1 Cortical bone tissue**

Compact bone tissue is a type of connective tissue. This is located in the outermost layer of the bones just below the periosteum. Bones are surrounded by a layer of connective tissue, the periosteum, into which tendons and ligaments attach (Reilly & Burstein, 1974).

#### **4.5.2 Spongy bone tissue**

Cancellous bone is characterized by being porous, forming interstitial sheets called sponge-like trabeculae. These plaques form a spongy structure in which holes filled with red bone marrow are interspersed.

Cancellous bone represents 20% of total bone mass and is found at the ends or epiphyses of long bones and the interior of other bones (Lindahl, 1976).

#### ***4.6 vertebral disc***

The intervertebral discs correspond to each of the pads that separate the vertebrae of the spinal column. These form a cartilaginous cushion which allows the mobility of the spine (González Martínez et al., 2017).

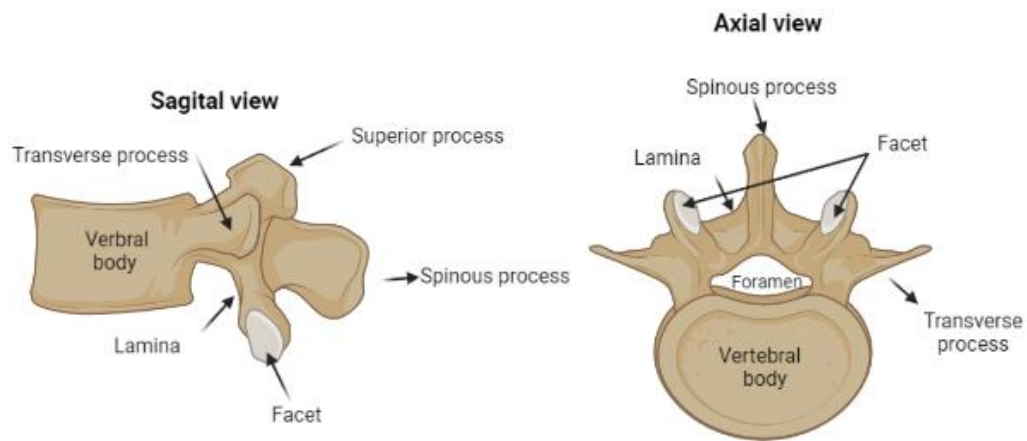


*Figure 12.* Parts of a vertebra. Own elaboration from Kardong (2007)

The purpose of this work is to contribute and offer a safe, easy and effective tool when it comes to providing information on biomechanics, the force points in the different areas of the spine, and quantifying the place of lumbar damage. Additionally, the simulation generates an optimal model of the individual's pathology to be analyzed, generating quantitative data on the pressure placed on the study surfaces, contributing significantly and providing a vast amount of information necessary to offer an ideal treatment as a solution to the pathology of the study object.

## 5. PROBLEM STATEMENT

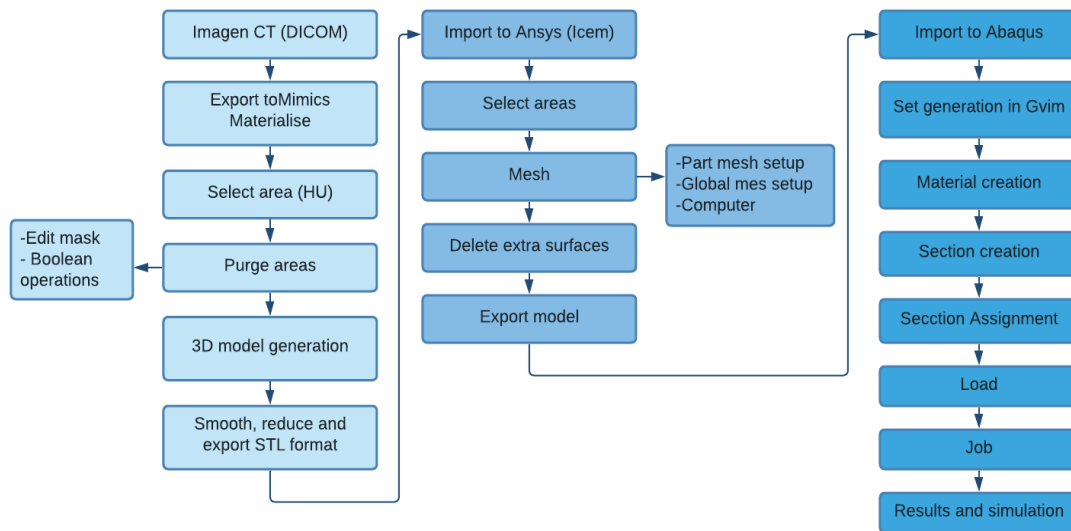
The inconveniences associated with the spine especially in the lumbar region have increased considerably in recent years. In that sense, the current teleworking modality generated by the new lifestyle adopted by COVID 19, has generated that a large part of the population maintains a bad posture of the spine, causing in addition to pain, several problems in the future such as scoliosis, osteophytes, vertebral deviation, among the most relevant affectations. These pathologies can be present from an early age, since in many cases their origin is genetic, while in other cases it is due to the individual's poor posture or incorrect loading postures. In addition, the population that is in heavy work where a load of material is essential is prone to developing these pathologies. On the other hand, sedentary individuals with considerable weight are also prone to having this disease. Currently worldwide, about 3% of the population suffers from some type of scoliosis (Scoliosis - Symptoms and causes - Mayo Clinic ", 2021).

Additionally, pathologies such as disc calcification, osteoporosis, osteopenia, among others, usually accompany the pathology of scoliosis because it largely degenerates in the bone and surrounding tissues (Haddas et al., 2019). Likewise, it is the cause of intense pain and serious problems in the biomechanics of the individual, mainly affecting the patient's gait and his independence when moving. In advanced degrees and if they do not have any treatment, it could greatly affect the vertebral disc causing a total wedging and affecting the spinal cord (Rittmeister et al., 1999). It is for this reason that an early diagnosis can greatly

improve the quality of life of the patient and significantly reduce pain and other associated pathologies.

## **6. METHODOLOGY**

For the creation of the resulting simulation, 4 different software were used: mimics materialise, Ansys (Icem), gVim y Abaqus. Additionally, it was essential to obtain a computed tomography (CT) whose format is Digital Imaging and Communication on Medicine (DICOM) of the object of study. Subsequently, the. dicom files were exported to the mimics materialize software, where a 3d model was built based on the images obtained from the CT. Next, the 3D model created in Mimics materialize was exported in a Standard Triangle Language format to create a 3d model (STL), this was imported into the second Ansys software (Icem) in which the meshing of the model was generated. Then, the model, once meshed, was imported into the Abaqus software, with which the simulation was carried out through the finite element method (FEM). Additionally, in this step, the gVim software necessary to create the sections or areas used in the model was used. Finally, the simulation of the model of the study subject was obtained.



*Scheme 2:* General methodology for obtaining the simulation. Own elaboration.

### ***6.1 Design and Implementation of the model in Mimics Materialize***

Mimics is a medical engineering software that allows you to efficiently create a 3D model and allows you to scale from research and development (R&D) to high volume clinical operations (Mimics, 2021).

As a first step, a 3D model was implemented through the Mimics Materialize software, for which it was necessary to obtain a computed tomography (CT) whose format is DICOM, which consists of 695 images, which were used to give it shape to the 3D model. Once the images are loaded, we proceed to choose a range of Heat units (HU) (see annex 2), which allows us to discard the range or areas that are not of interest to us. In this way, the range of HU used for modeling can be seen in table 2.

Once the areas are discarded, a much more detailed exclusion of the areas to be obtained is carried out, for which the area must be selected box by box of each section using

the *edit mask tools* (see annex 3). On the other hand, the Boolean operations tool was used to eliminate the masks, and thus obtain the required sections. In addition, for the formation of the model, the different views that it presents can be helped, such as the coronal, sagittal, and axial views. (see annex 1).

*Table 3.* HU range, according to the vertebral spine area. Own elaboration.

<i>Spinal area</i>	<i>HU range</i>
<i>Cortical bone</i>	164-1718
<i>Spongy bone</i>	148-1718
<i>Vertebral matrix</i>	86-196
<i>Intervertebral discs</i>	86-196

With the aforementioned tools, the sections consisting of a cortical, cancellous, vertebral nucleus, and fibrous rings were divided, thus obtaining the following regions, see *figure 13*.

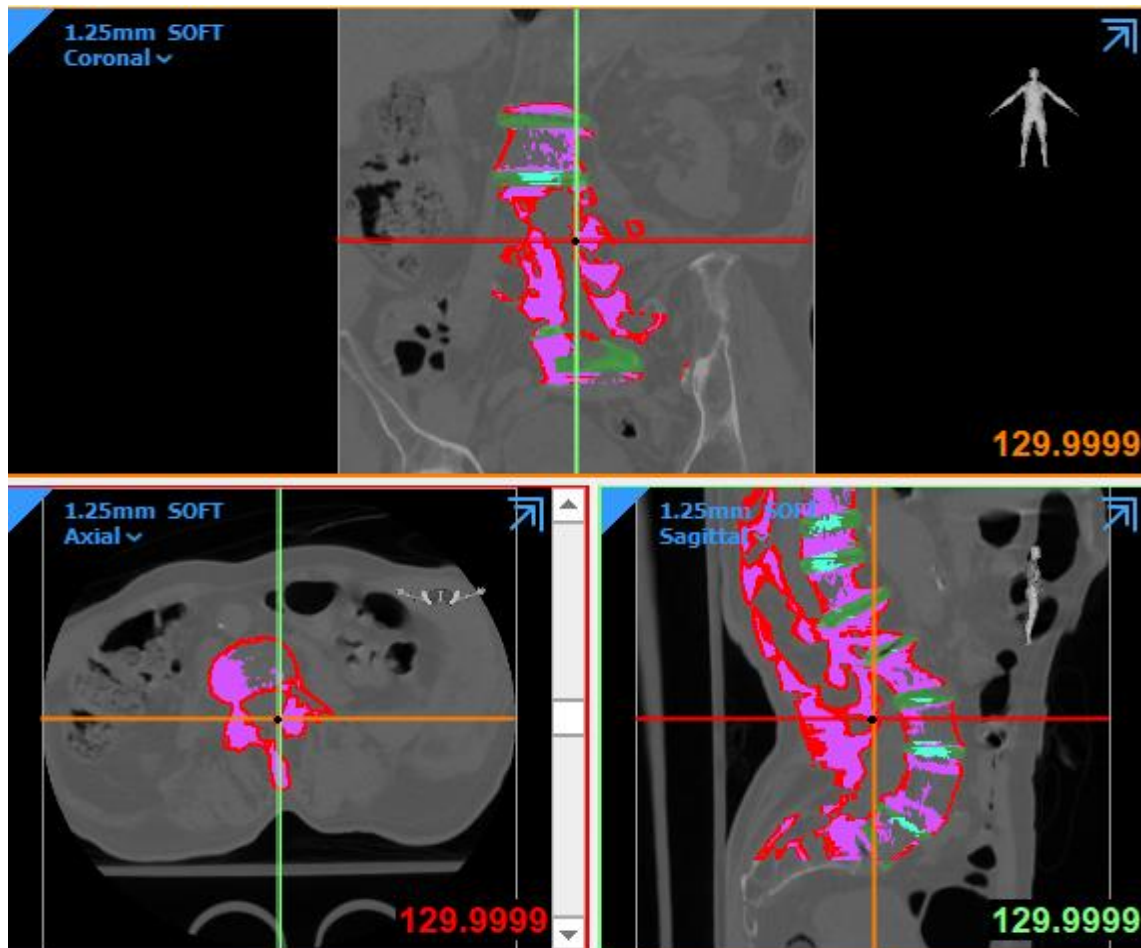


Figure 13. 3D model editing (red) cortical area, (purple) cortical area, (blue) vertebral nucleus, (green) fibrous rings. Own elaboration.

### 6.1.1 Creation of the 3D model with Mimics Materialize

Finally, the 3D model is divided into the 4 aforementioned sections. For this, the Boolean operation option was used (see annex 4). The reason for this division is to have a better analysis of the finite element method (FEM), to be able to observe in more detail how pressure and force affect each section. Additionally, the vertebral disc was divided into two sections, one of which encompasses its nucleus and the other in which all the fibers of the

disc are found. Due to the degree of calcification of the discs, it is not possible to make clear divisions.

Additionally, only the spinal area was taken, eliminating the ribs and the final area of the sacral vertebrae, focusing only on the most prominent area of scoliosis. Obtaining the following images and the final model.

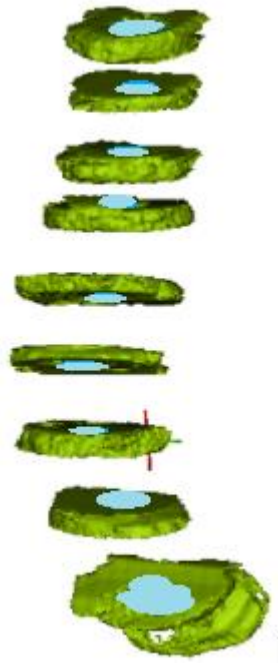


*Figure 14.* 3D model of intervertebral disc nucleus (green) and fibrous rings (white blue). Own elaboration.



*Figure 15.* 3D model of the spongy bone area. Own elaboration.

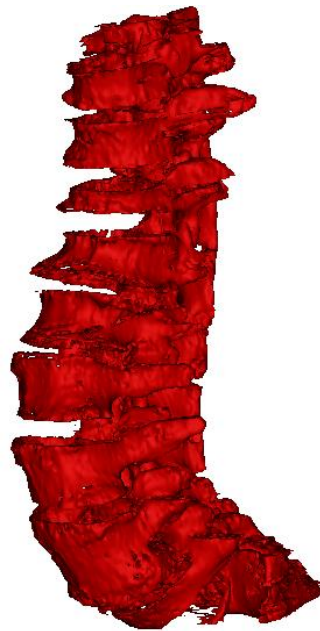


*Figure 16.* 3D model of the cortical bone area. Own elaboration.

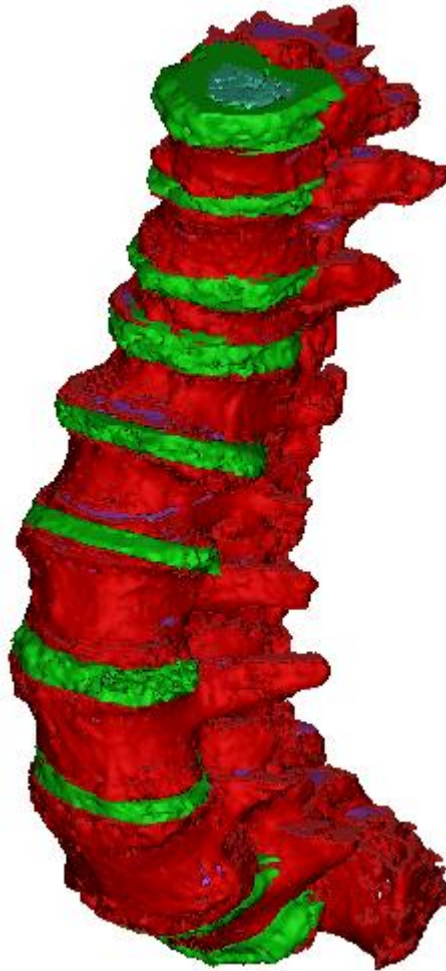
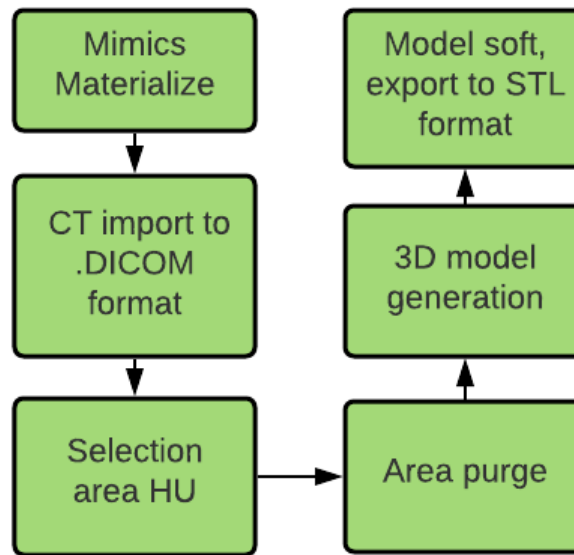


*Figure 17.* 3D model of the spine, last 3 dorsal vertebrae, and lumbar vertebrae. Vertebral discs (green), cancellous bone (purple), cortical bone (red). Own elaboration.

Finally, a smoothing of each section was carried out, establishing a smoothing factor of 0.75 to polish the surface without eliminating important details for the FEM study (see annex 5). Subsequently, the model was exported in Standard Triangle Language format to create a 3d model (STL) (see annexes 5, 6, and 7) which preserves the properties of the 3D model to be able to perform the meshing in the following program.



*Scheme 3.* 3D modeling general scheme. Own elaboration.

### **6.2 Ansys Mesh Design (ICEM)**

ANSYS, (Swanson Analysis Systems, Inc.) is software based on finite elements and computational fluid dynamics. In addition, it is a strong simulator for creating simulations aimed at predicting how a certain product will work and react under a real environment. (Ansys, 2021)

For the implementation of the meshing, the model was exported to the Icem program (Ansys), the format to be used as the STL. Once the design was exported, the model meshed where the parameters to be used were the following:

*Table 4.* Values obtained through simulation in the Ansys (Icem) program. Own Elaboration.

<i>Area</i>	<i># of elements</i>	<i>Layers</i>	<i>Nodes</i>
<i>Spongy bone</i>	44403	10000	16359
<i>Cortical bone</i>	66642	10000	38288
<i>Vertebral matrix</i>	17688	1000	2751
<i>Fibrous rings</i>	12860	1000	3475
<b><i>Total</i></b>	141593	22000	60873

Once the meshing was computed, the divisions of each section were made manually to obtain the four desired sections, this was done with the addition to the part tool (see annex 9), which allows joining more than one block of meshes. Giving as a result the following meshing sees *figure 18*.

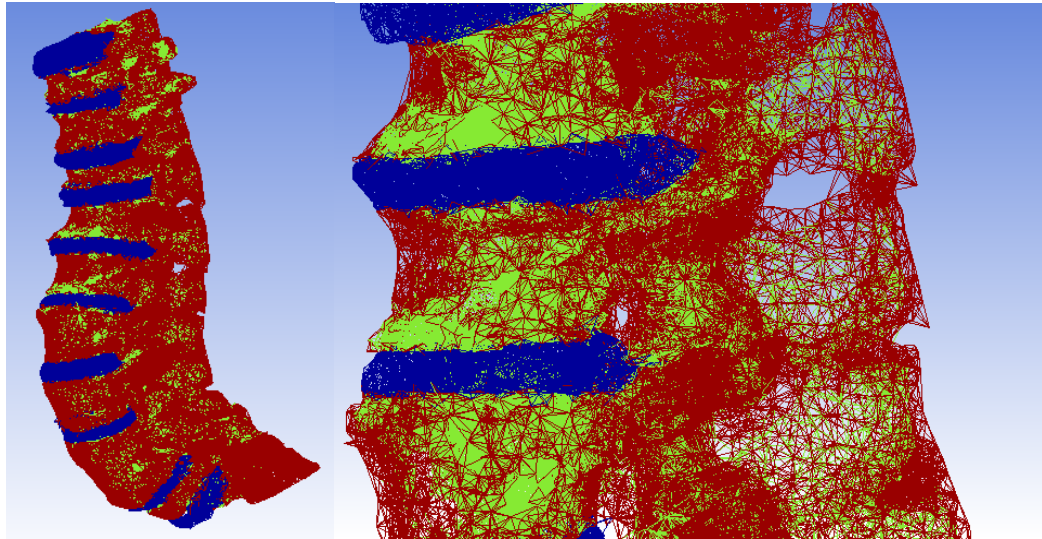
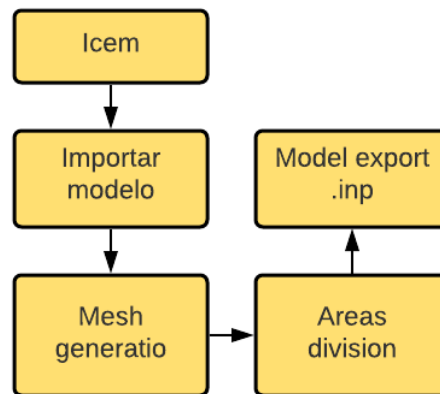


Figure 18. Meshing the model in Ansys (Icem). Own elaboration.

Finally, the model obtained was exported in .inp format (see annex 10,11,12), since it is compatible with Abaqus.



Scheme 4. The meshing of the general scheme model. Own elaboration.

### ***6.3 Finite element analysis in Abaqus***

Finite element analysis or FEM was created to solve structural calculation problems, ranging from fields such as engineering to fluid mechanics, heat diffusion, pressure simulations, force, humidity, and temperature in structures of all kinds (Upct, 2013).

For our case, in particular, the finite element analysis through the Abaqus program will allow us to know in greater depth certain variables of interest such as force, weight, the pressure of the patient, and their pathological affectation, in such a way that allows us to know their future impact.

In addition, it will allow us to observe the affected structures in more detail and to know quantitatively the tensions in each study area (Wang et al., 2014).

#### ***6.3.1 Sets creation***

Vim is a highly configurable text editor built to make creating and changing any type of text very efficient. Additionally, it is compatible with various formats including .inp (Vim online, 2021).

The gVim program was used, which is a text editor. And the creation of SETS was carried out to be able to select the desired area. (see complete code in annex 18)

```

...
*Part, name=PART-1
*Node
+--73130 lines: 1, -9.62534904, 29.417305, 112.176956-----
*Element, type=S3
+--26754 lines: 1, 1524, 6629, 6633-----
*Element, type=C3D4
+--239364 lines: 137785, 23544, 32913, 55246, 25346-----
*Elset, elset=CORTICAL_ELSET
+--8843 lines: 137785, 137786, 137788, 137790, 137791, 137792, 137795, 137796, 137799, 137800, 137801, 137803, 137806, 137807, 137809-----
*Elset, elset=DISCOS1_ELSET
+--452 lines: 7213, 7214, 7215, 7216, 7217, 7218, 7233, 7234, 7235, 7275, 7279, 7302, 7303, 7304, 7305, 7306-----
*Elset, elset=DISCOS_2_ELSET
+--1221 lines: 1, 2, 3, 4, 5, 6, 7, 8, 9, 10, 11, 12, 13, 14, 15, 16-----
*Elset, elset=ESPONJOSO_ELSET
+--6119 lines: 137789, 137793, 137794, 137797, 137798, 137802, 137804, 137805, 137808, 137815, 137824, 137826, 137827, 137828, 137829, 137834-----
*End Part

```

Figure 19. Code for creating Sets in Gvim. Own elaboration.

### 6.3.2 Material creation

In the present model, four different materials were used, depending on the focus area. That is a material for the cortical, cancellous area, vertebral nucleus, and fibrous rings.

Additionally, the elastic property was selected for each material (see annex 15), due to its properties, for which the data from table 4 was used for the values of Poisson's ratio and Young's modulus.

#### 6.3.2.1 Young's Modulus and Elasticity

- Young's modulus: it is related to the mechanical properties of solid, elastic, and linear materials. This defines the relationship between the deformation of the material and the stress, that is, the force applied per unit area. (Kurutz & Oroszváry, 2010) In our particular case, we will focus on the tensions of:
  - Von Mises: This refers to the energy of distortion, that is, the deformation of a solid due to its internal energy (Fouad, 2010).

- Maximum principal stress: It focuses on analyzing the maximum stress of the material, obtaining the distortion energy, in which if the stress is outside the range, the deformation of the material remains over time (Eser et al., 2013).
- Poisson's ratio: It is a dimensionless quantity, characteristic of each material. Considered as an indication of the deformation of a piece of material before the application of certain forces (Reis et al., 2020).

To obtain the values corresponding to the mechanical (elastic) characteristic of the material, in our case the following values for Young's modulus and elasticity were obtained from the literature (see annexes 13 and 14).

*Table 5:* Data for Finite element model of functional spinal units FSU. Own elaboration from (Kurutz, M., & Oroszváry, L. 2010).

<i>Area</i>	<i>Young's modulus (MPa)</i>	<i>Poisson</i>
<i>Cortical</i>	12000	0.3
<i>Spongy</i>	150	0.3
<i>Vertebral matrix</i>	9	0.4
<i>Fibrous rings</i>	5.5	0.45

### ***6.3.3 Secciones creations***

For the model, it was used as solid-homogeneous properties and subsequently, the material previously created for each area of the model was selected. Also, it can be noticed that as each section is created the selected area will change color as shown in *figure 20*.

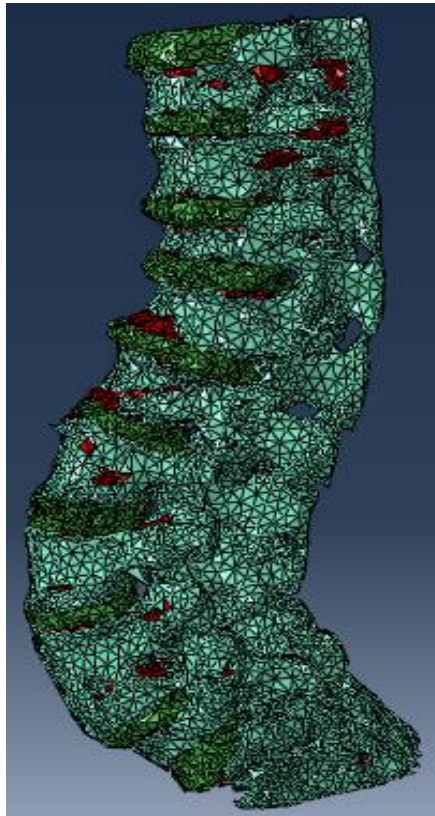


*Figure 20.* Creation of the sections in Abaqus. Own elaboration.

### ***6.3.4 Seccion Assignment***

For the assignment of each section, the previously created set was selected, which contains the section and the material for each area (see annexes 16 and 17).

### 6.3.5 Loads

As a next step, the embedding section was established where the translation and rotation of the model along the x, y, and z axes are considered. (Defining a base motion boundary condition, 2021). Those are the boundaries conditions of the model. In other words, the base of our model is located at the bottom of the design as shown in fig. 21. For which, the option is seen in fig. 19. In which, it tells us the following:  $U1 = U2 = U3 = UR1 = UR2 = UR3 = 0$ . This means that the model is fully incorporated in the x, y, z plane.



Figure 21. Total embedment. Own elaboration.

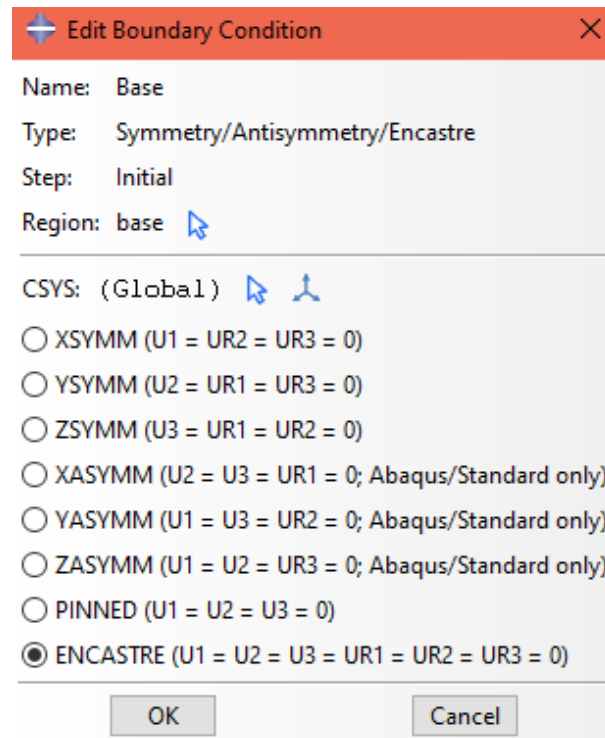


Figure 22. Embedding interface. Own elaboration.

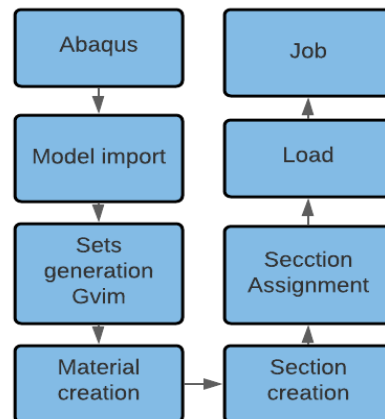
The pressure values for each study area were taken from the literature focusing on the 'up' position of the individual, this pressure value is 0.43 MPa (Mörl et al., 2020).

### 6.3.6 Simulation

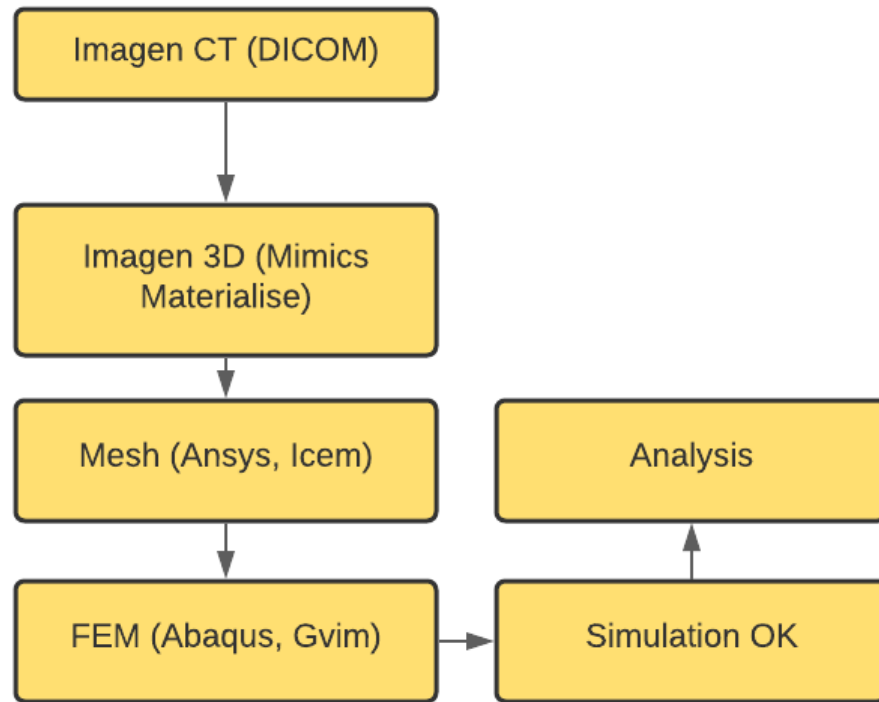
In the final phase that corresponds to the simulation, a work order was generated in the Abaqus software, which will analyze the parameters previously entered, such as type of material, selected insert, type of loads, and place of the same. It should be taken into account that, as it is a fairly extensive model, the average time to generate the simulation is around 7 hours.

### 6.3.6.1 Interface and mechanisms

The simulation obtained presents a range of visualizations, among the most relevant for our research and our model, are the primary and the deformed model; Von Mises's analysis, and main maxim. Additionally, simulation is supported with a video model, which is very important in the analysis of the design, because, through this, the importance of generating a model based on the study of finite elements, such as adjuvant for surgical viability. In addition, the simulation provides relevant data such as the areas or zones in which there is greater bone damage, be it cortical, cancellous, or discs, which is essential to determine in more depth the affectation and degree of the pathology. On the other hand, it is also very important to know the specific area of greatest pressure and stress to improve rehabilitation techniques and methods.



*Esquema 5.* Generation of the simulation in Abaqus. Own elaboration.



*Esquema 6.* General model for obtaining the simulation. Own elaboration.

## 7. RESULTS

Once the simulation was finished, we observed the following results:

We note a relevant difference between the original model and its deformation as shown in *figure 23*. The plane of greatest deformation was determined in the sagittal plane.

Observing *figures 23 and 24* that correspond to the section of the cortical area, it can be highlighted that the areas colored in white, whose Von Mises values are found with values of  $1.62 \text{ e} + 1 \text{ MPa}$ , are those areas most prone to bone fracture. (see annex 21)

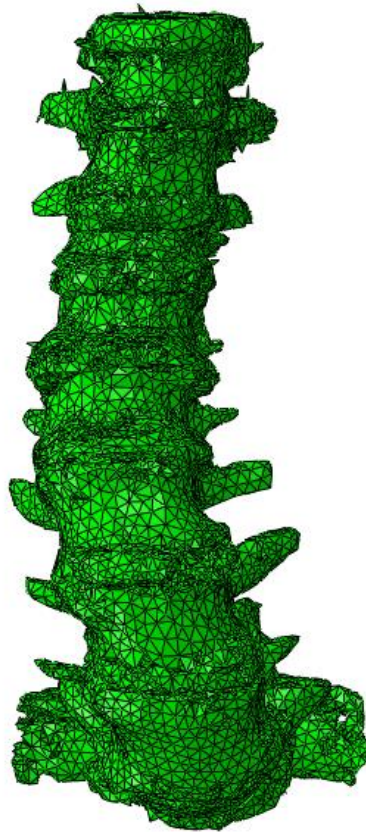


*Figure 23.* Original model. Own elaboration.

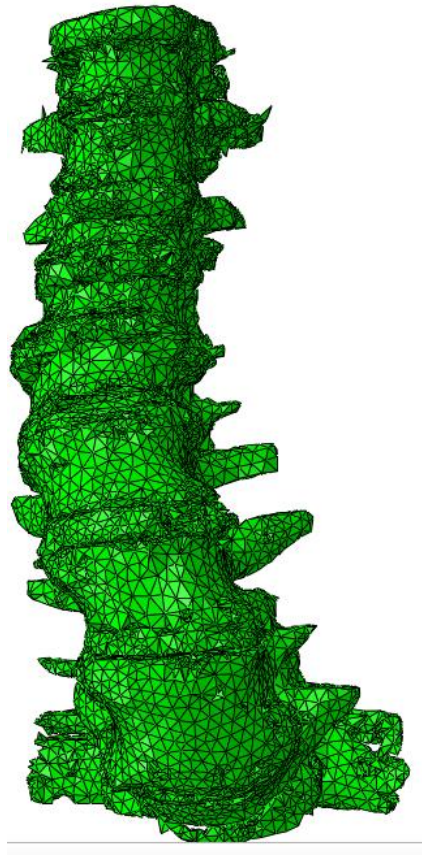


*Figure 24.* Deformed modelo. Own elaboration.

On the other hand, focusing on the area of cancellous bone figure 25 and 26, which corresponds to the innermost area of the bone characterized by trabeculae or sponge-shaped spaces (Nikoghosyan et al., 2019). It can be noted that, as in the cortical bone area, the area most prone to a load-bearing fracture.

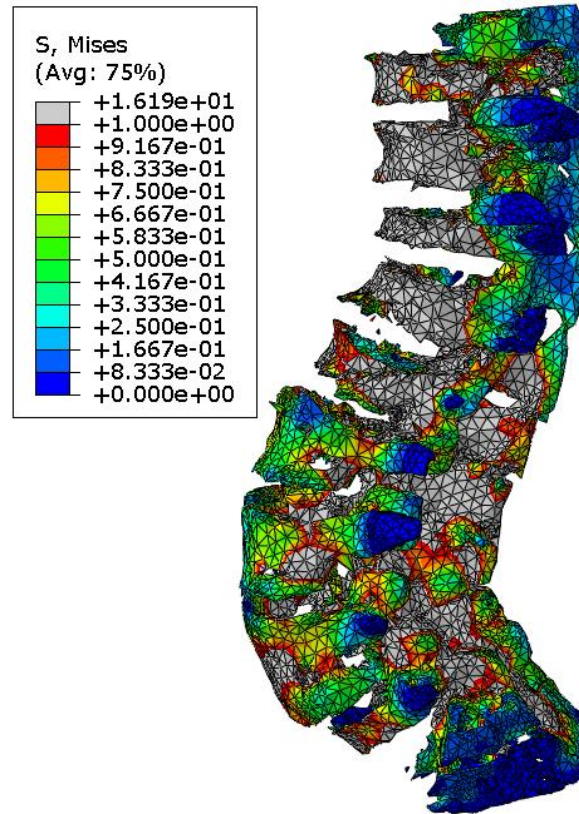


Figure 25. Von Mises of cortical area. Own elaboration.

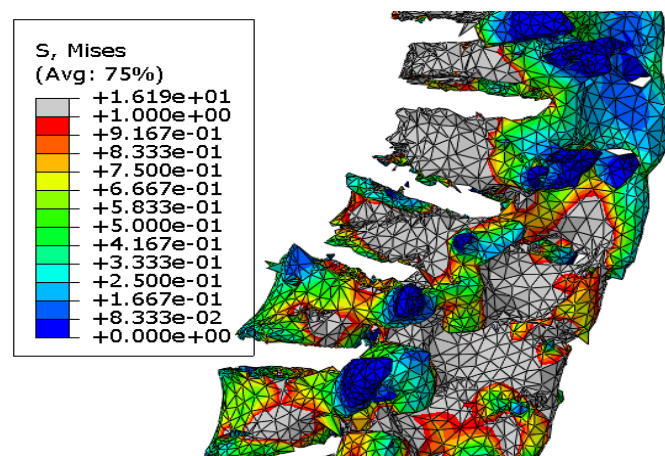
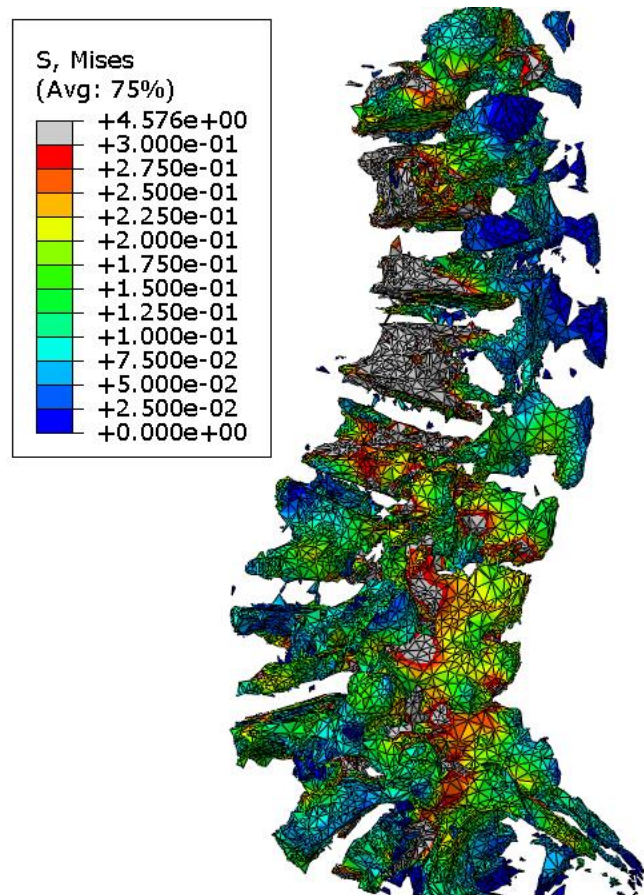


Figure 26. Von Mises close-up of the cortical area. Own elaboration.

The vertebral discs whose areas mainly studied in this model are: the vertebral nucleus and the fibrous rings see *figure. 27*. In the area of vertebral discs, it can be noted that the maximum Von Mises value is  $1.44 \text{ e } + 1$  see *figure 27* until *figure 30*, being only below the value of the cortical bone.



*Figure 27.* Von Mises spongy area. Own elaboration.

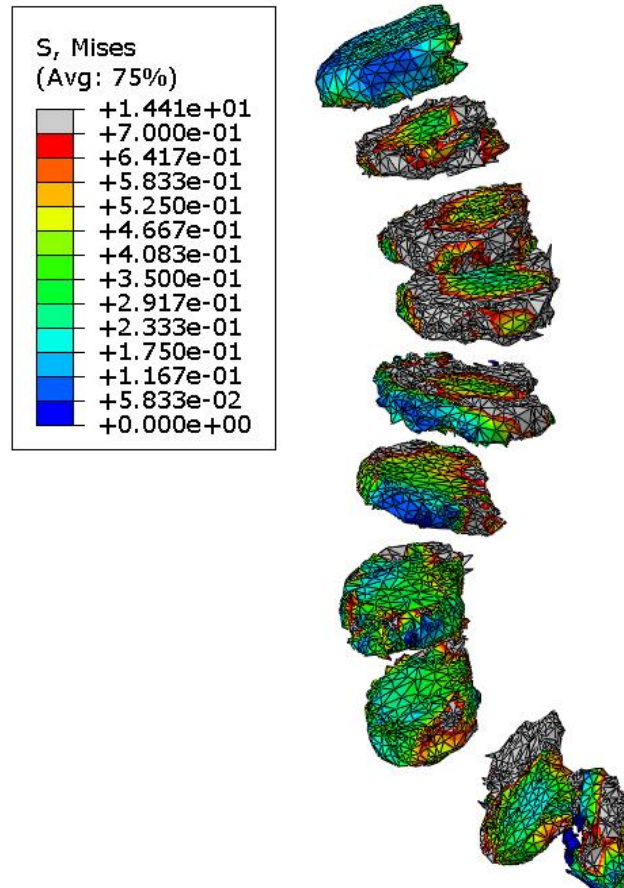


Figure 28. Von Mises intervertebral area. Own elaboration.

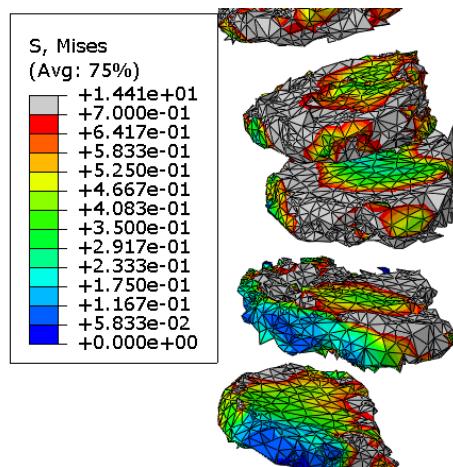


Figure 29. Von Mises intervertebral area approach. Own elaboration.

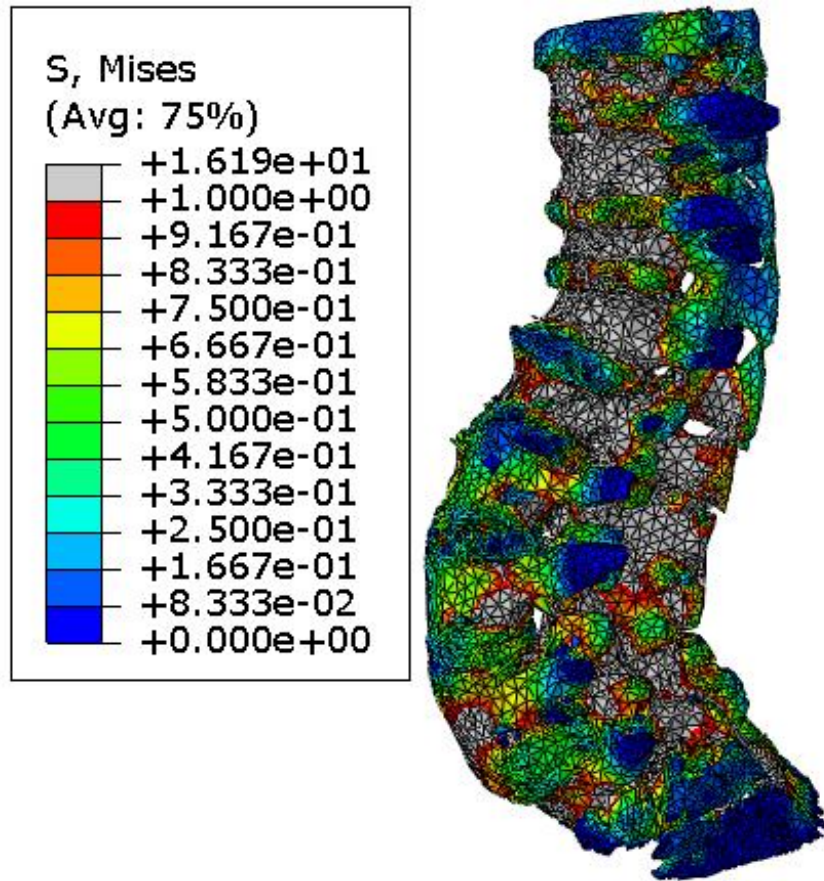


Figure 30. Von Mises general model. Own elaboration.

Table 6. Von Mises maximum value in each study area. Own elaboration.

<i>Area</i>	<i>Value max de s, miss (MPa)</i>
<i>Cortical</i>	1.62 e+1
<i>Spongy</i>	4.58
<i>Vertebral discs (matrix, fibrous rings)</i>	1.44 e+1

While the region of the vertebral disc area that corresponds to both the nucleus and the fibrous rings has a value below the cortical area.

*Table 7.* Displacement distance between the original and deformed model. Own elaboration.

<i>Area</i>	<i>Magnitude</i>
<i>Original model</i>	4.59791e+01
<i>Deformed model</i>	6.40807e+01

The displacement distance of the model concerning the original is  $1.81016e + 01$ , taking the x-plane as a reference. (see annexes 19 and 20)

Finally, one of the most relevant analyzes for our study model is that of the maximum principal stress, which tells us that if the pressure applied to the material is greater than the maximum value, the material undergoes a permanent deformation in the body. As shown in *figure 31*, the places of permanent deformation are those that are found mainly in the spinous process area in the lumbar region.

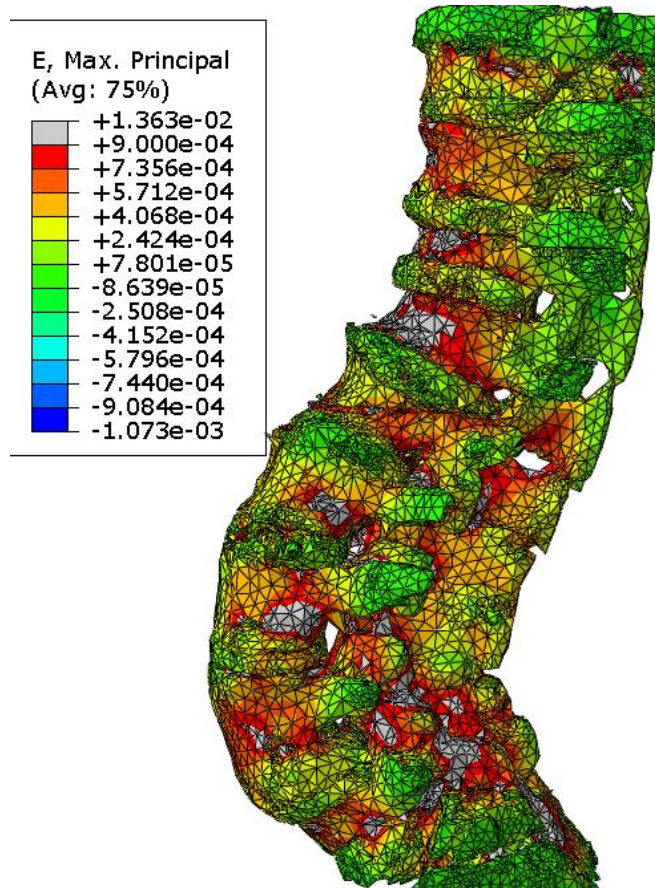


Figure 31. Maximum principal stress of the generated model. Own elaboration.

## 8. DISCUSSION

Scoliosis has become in recent years one of the most common pathologies characterized by spinal pain due to a poor distribution of body weight. If this condition is not treated early, it can worsen over time. This is the reason for the importance of the study, which shows us in detail each specific area of the stress and pressure analysis in each region, providing qualitative values.

Analyzing the cortical zone, it can be said that a prominent angulation is observed in the lumbar area, causing greater vertebral wedging. On the other hand, it is important to mention that in the lower thoracic area between T10 and T12 there is a peripheral increase in osteophytes, this is due to the angulation in the lumbar area previously mentioned, these results agree with the investigations of (Sun et al., 2018).

In addition, in our deformed model, we can notice bone splinters caused by pressure, as well as bone deformation, a deformation that is similar in previous models by other authors such as (Simon et al., 2018). It should be noted that the simulated model in this work only focuses on the 'raised' position of the subject because this presents a greater pressure than other positions and due to the poor distribution of body weight due to spinal dystrophy caused by scoliosis this is the area with the highest probability of fracture.

Additionally, the Von Mises analysis determines if the material in this case the vertebral spine will yield or fracture, showing quantitative values of the most affected areas. In addition, in the cortical area, especially in the lower lumbar region, there is considerably wedging in the area of the spinous process, from the T9 to L5 vertebrae, focusing on the peripheral area of the vertebral body in the case of the thoracic vertebrae. and in the spinous process, in the case of the lumbar vertebrae, causing a severe degree of atrophy in these areas, causing immobility to the study subject, this analysis is analogous to the observations made by (Been & Kalichman, 2014).

Additionally, the model presents mostly areas prone to load fracture, this can be noted by the value given in each region that ranges from  $2.5e^{-1}$  to  $1.62e^{+1}$  mostly, these results agree with the research de (Sabo et al., 2017) In addition, the areas with the lowest load are concentrated in the lower part of the lumbar spine. On the other hand, the T12 and L1 vertebrae present a high degree of deformation wedging the intervertebral disc and producing a greater degree of osteophytes in the area (Fig. 25), these results are analogous to the studies of (Him et al., 2016).

On the other hand, in the region corresponding to the cancellous bone it can be noted that, as in the area of cortical bone, the area most prone to a load-bearing fracture corresponds to the periphery of the vertebral body of the thoracic vertebrae and the area of the apophysis. spiny of the lumbar vertebrae. However, the spongy area has a greater range of performance

because several areas can be found in which the performance is lower. This analysis agrees with the research conducted by (Chen et al., 2020).

In a healthy individual, the intervertebral region is composed of cartilage, but in the case of our study subject, it presents a strong calcification of discs, which is evident in our model. For this reason, the maximum value of  $\sigma_{\text{mises}}$  is higher than the spongy tissue and, like the cortical area, since it is a compact tissue caused by calcification, this area is prone to have lower performance and therefore fractures. As can be seen in the research of (Sabo et al., 2017).

In addition, the individual presents osteoporosis, which suggests that the trabeculae of the spongy tissue expand which causes this area to be very fragile, for this reason, the index of  $\sigma_{\text{mises}}$  is lower, which indicates that with a reduced load value the material is easily deformable. This is analogous to the studies of (Routh et al., 2005)

Finally, in the area of vertebral discs, we cannot speak of a fracture as such since the composition of the material is not bone but cartilage, which is why it shows severe wedging in the thoracic vertebrae, mostly in the peripheral area that is expanding to the central area. which is close to the intervertebral nucleus, having in this area a maximum of  $1.44 \times 10^1$  (Fig. 28) the results agree with the research of (Braun et al., 2006).

Generally speaking, the model presents a strong wedging of discs especially in the thoracic region, as well as severe atrophy of the spinous processes of the lumbar vertebrae. In the results phase, it is noted that the areas that are outside the stress limit for both the Von

Mises analysis and the maximum principal stress, are found in the dorsal region, in the area of the vertebral body, while in the region lumbar maximum stress is in the spinous process area.

Therefore, the simulated model allows us to know with certainty the most affected areas as a preclinical adjunct so that the treating physician can offer more appropriate treatment or even predict the need to treat the condition with surgery or, if not, improve the condition. by other methods. as can be seen in the project of (Coombs et al., 2011)

Additionally, the study has a close relationship between the points of greatest pressure and vertebral damage. This is analogous to the study by Kim et al. which states that there is a close relationship between nerve root stress and the scoliotic curve (Kim et al., 2009). In other words, a wedging of discs or vertebrae is greater depending on the scoliotic curvature. (see annexes 22 and 23).

On the other hand, several studies analogous to the subject indicate that the reduction, "configuration, of force, can be used to reduce a scoliotic curve" (Taghi et al., 2016). This allows us to infer that the implementation of rehabilitation or exercises can serve as an adjunct to improve the strength and pressure points in the different areas, which would reduce the scoliotic curve, improving people's quality of life. Additionally, the model provides us with data such as the level and place of greatest calcification, which allows a clearer picture of the individual's pathologies, as well as the techniques of how to alleviate pathologies, as can be seen in the research of ( Gonzalez Alvarez et al., 2018).

On the other hand, the surgical feasibility can be determined or even accompany the simulation with implant techniques that could be simulated in the model in order to determine the best material and area to alleviate or improve the pathology, as well as see the specific areas for placement. implants and establish an improvement in body weight distribution.

## 9. Conclusion

It can be concluded that the simulation obtained with Abaqus through FEM is a very useful method for generating a fairly detailed 3D model that allows determining the number of parameters such as areas of stress, tension, specific pressures, areas of calcification or decalcification of bone, among others. This allows early prediction of the damage that the spinal column may suffer to determine a surgical need. Additionally, it should be taken into account that to obtain a detailed model the computed tomography must be quite sharp since in this way when generating the 3D model, meshing, and final simulation, the design noise will be filtered as long as the files.

DICOM comes in the highest quality. On the other hand, the model allows us to quantitatively identify the specific place of lumbar damage, as well as the model, provides the specific sites of vertebral damage as a function of time, thus, it can be determined that the area most prone to fracture damage and/or wedging is the intervertebral area since analyzing the results it is concluded that the disc area, especially the fibrous rings, present a high degree of calcification, so over time, it will suffer a wedging almost completely, which may obstruct the spinal cord and cause irreparable harm to the patient.

On the other hand, it can be said that in our particular model the study individual must undergo surgery as soon as possible because the analysis in the simulation indicates that the stress caused by the load is higher than the maximum level, causing a deformation. permanent in the subject.

Finally, it is concluded that the simulation obtained through the analysis of finite elements is an easy, practical, and low-cost method as a complement to predict damage in

specific areas of the human body as well as to establish parameters to reduce damage to the spine. through the improvement of habits. In addition, it is a great ally in medical studies since it provides several data on the composition and behavior of tissues or specific areas in the study.

## **10. Recommendations and Limitations**

It is recommended to provide all the necessary data, as well as the information of the study subject to ensure that the simulation is as accurate as possible among the data and necessary information are patient's pathology, body weight, height, sex, computerized tomography files in high resolution to generate modeling with the least possible noise, bone densitometry files these to know the internal state of the bone calcification of each study area. Generate a study of preferred pressure areas for each anatomical position. Additionally, a study of pressure in the biomechanics of gait to know in a general way the distribution of body weight. In addition, it is recommended to generate the simulation on a state-of-the-art computer because, depending on the area, number of nodes, and elements created in the mesh, the simulation can take several hours or even days. Finally, it is recommended that, since it is an experimental method, the analysis is reaffirmed with a health professional or with conventional methods to give a diagnosis or treatment to the pathology.

On the other hand, the limitations of the present study include that in order to have a better model over time and to correlate with the simulation, a CT should be used to correlate the data. In addition, how to complement the results obtained as well as the discussions, it would be ideal to carry out the study in different models taking into account age, sex and regional factors such as race and place of birth, as well as sedentary lifestyle or physical activity carried out by the object of study.

## 11. Future work

As a continuation of this thesis work and as in any other research project, various lines of research remain open and in which it is possible to continue working. During the development of this thesis, some future lines have emerged that have been left open and that they are expected to attack in the future; Some of them are more directly related to this thesis work and are the result of questions that have arisen during the completion of the thesis.

Others are more general lines that, however, are not the subject of this thesis; These lines can be used to retake them later or as an option for future work for other researchers. Below are some future works that may be developed as a result of this research or that, due to exceeding the scope of this thesis, have not been able to be treated in sufficient depth.

In addition, some specific developments are suggested to support and improve the proposed model and methodology. Possible future jobs include:

- It is proposed to carry out a supplement with implants as a surgical treatment for quite severe pathologies, establishing a preclinical study of the best material for the implant (s), as well as the areas for their placement.
- Optimize the generation of the 3D model to reduce the simulation creation time.

## 12. References

1. *ABAQUS Student Edition*. (s/f). 3Ds.com. Recuperado el 12 de septiembre de 2021, de <https://edu.3ds.com/en/software/abaqus-student-edition>
2. Abul-Kasim, K., Overgaard, A., Maly, P., Ohlin, A., Gunnarsson, M., & Sundgren, P. C. (2009). Low-dose helical computed tomography (CT) in the perioperative workup of adolescent idiopathic scoliosis. *European Radiology*, *19*(3), 610–618. <https://doi.org/10.1007/s00330-008-1178-4>
3. Aebi, M. (2005). The adult scoliosis. *European Spine Journal*, *14*(10), 925–948. <https://doi.org/10.1007/s00586-005-1053-9>
  - a. Ahmadi, H., & Salehani, Y. E. (2007). A Modified Version of SNOW2 . 0. *Electronic Engineering*, February, 20–22.
4. Ansys.com. Recuperado el 12 de septiembre de 2021, de <https://www.ansys.com/news-center/press-releases/ansys-2021-r2-accelerates-engineering-exploration-collaboration-automation>
5. Arlet, V., Odent, T., & Aebi, M. (2003). Congenital scoliosis. *European Spine Journal*, *12*(5), 456–463. <https://doi.org/10.1007/s00586-003-0555-6>
6. Been, E., & Kalichman, L. (2014). Lumbar lordosis. *Spine Journal*, *14*(1), 87–97. <https://doi.org/10.1016/j.spinee.2013.07.464>
7. Braun, J. T., Hoffman, M., Akyuz, E., Ogilvie, J. W., Brodke, D. S., & Bachus, K. N. (2006). Mechanical modulation of vertebral growth in the fusionless treatment of progressive scoliosis in an experimental model. *Spine*, *31*(12), 1314–1320.

<https://doi.org/10.1097/01.brs.0000218662.78165.b1>

8. Chen, X., Cai, H., Zhang, G., Zheng, F., Wu, C., & Lin, H. (2020). The construction of the scoliosis 3D finite element model and the biomechanical analysis of PVCOR orthopaedy. *Saudi Journal of Biological Sciences*, 27(2), 695–700.  
<https://doi.org/10.1016/j.sjbs.2019.12.005>
9. *Defining a base motion boundary condition*. (s/f). Recuperado el 12 de septiembre de 2021, de <https://abaqus-docs.mit.edu/2017/English/SIMACAECAERefMap/simacae-tlbibceditorsbasemotion.htm>
10. Diab, K. M., Sevastik, J. A., Hedlund, R., & Suliman, I. A. (1995). Accuracy and applicability of measurement of the scoliotic angle at the frontal plane by Cobb's method, by Ferguson's method and by a new method. *European Spine Journal*, 4(5), 291–295. <https://doi.org/10.1007/BF00301037>
11. Eser, A., Tonuk, E., Akca, K., Dard, M. M., & Cehreli, M. C. (2013). Predicting bone remodeling around tissue- and bone-level dental implants used in reduced bone width. *Journal of Biomechanics*, 46(13), 2250–2257.  
<https://doi.org/10.1016/j.jbiomech.2013.06.025>
12. Fouad, H. (2010). Effects of the bone-plate material and the presence of a gap between the fractured bone and plate on the predicted stresses at the fractured bone. *Medical Engineering and Physics*, 32(7), 783–789.  
<https://doi.org/10.1016/j.medengphy.2010.05.003>
13. Gallinas, F., Garatea, M., Solís, B., Duarte, J., Pediatría, S. De, & Virgen, H.

- (2004). *C d i c d c*. 50–52.
14. Gonzalez Alvarez, A., Dearn, K. D., Lawless, B. M., Lavecchia, C. E., Vommaro, F., Martikos, K., Gregg, T., & Shepherd, D. E. T. (2018). Design and mechanical evaluation of a novel dynamic growing rod to improve the surgical treatment of Early Onset Scoliosis. *Materials and Design*, 155, 334–345.  
<https://doi.org/10.1016/j.matdes.2018.06.008>
  15. González Martínez, E., García-Cosamalón, J., Cosamalón-Gan, I., Esteban Blanco, M., García-Suarez, O., & Vega, J. A. (2017). Biology and mechanobiology of the intervertebral disc. *Neurocirugia*, 28(3), 135–140.  
<https://doi.org/10.1016/j.neucir.2016.12.002>
  17. Haddas, R., Xu, M., Lieberman, I., & Yang, J. (2019). Finite Element Based-Analysis for Pre and Post Lumbar Fusion of Adult Degenerative Scoliosis Patients. *Spine Deformity*, 7(4), 543–552. <https://doi.org/10.1016/j.jspd.2018.11.008>
  18. Him, S., Wong, J., Chiu, K. Y., & Yan, C. H. (2016). *V24I3P403*. 24(3), 403–410.
  19. Kardong, Kenneth V. (cop. 2007). *Vertebrados anatomía comparada, función, evolución* (4a ed edición). McGraw-Hill / Interamericana de España
  20. Karimi, M. T., Rabczuk, T., & Pourabbas, B. (2020). Evaluation of the efficiency of various force configurations on scoliotic, lordotic and kyphotic curves in the subjects with scoliosis. *Spine Deformity*, 8(3), 361–367.  
<https://doi.org/10.1007/s43390-020-00072-x>
  21. Kim, H. J., Chun, H. J., Kang, K. T., Lee, H. M., Kim, H. S., Moon, E. S., Park, J. O., Hwang, B. H., Son, J. H., & Moon, S. H. (2009). A validated finite element

- analysis of nerve root stress in degenerative lumbar scoliosis. *Medical and Biological Engineering and Computing*, 47(6), 599–605.  
<https://doi.org/10.1007/s11517-009-0463-y>
22. Kim, J. M., & Bixel, M. G. (2020). Intravital Multiphoton Imaging of the Bone and Bone Marrow Environment. *Cytometry Part A*, 97(5), 496–503.  
<https://doi.org/10.1002/cyto.a.23937>
23. Kittleson, C., & Lim, W. (n.d.). *the most ac- The. i.*
24. Kurutz, M., & Oroszváry, L. (2010). Finite element analysis of weightbath hydrotraction treatment of degenerated lumbar spine segments in elastic phase. *Journal of Biomechanics*, 43(3), 433–441.  
<https://doi.org/10.1016/j.jbiomech.2009.10.004>
25. Kyung, H. K., Jeong, Y. P., & Dong, K. C. (2009). Fusion criteria for posterior lumbar interbody fusion with intervertebral cages: The significance of traction spur. *Journal of Korean Neurosurgical Society*, 46(4), 328–332.  
<https://doi.org/10.3340/jkns.2009.46.4.328>
26. Lindahl, O. (1976). Mechanical properties of dried defatted spongy bone. *Acta Orthopaedica*, 47(1), 11–19. <https://doi.org/10.3109/17453677608998966>
27. Lowe, T. G., Edgar, M., Margulies, J. Y., Miller, N. H., Raso, V. J., Reinker, K. A., & Rivard, C. H. (2000). Etiology of idiopathic scoliosis: Current trends in research. *Journal of Bone and Joint Surgery - Series A*, 82(8), 1157–1168.  
<https://doi.org/10.2106/00004623-200008000-00014>
28. Materialise.com. Recuperado el 12 de septiembre de 2021, de

<https://www.materialise.com/en/medical/mimics-innovation-suite/mimics>

29. Mörl, F., Günther, M., Riede, J. M., Hammer, M., & Schmitt, S. (2020). Loads distributed in vivo among vertebrae, muscles, spinal ligaments, and intervertebral discs in a passively flexed lumbar spine. In *Biomechanics and Modeling in Mechanobiology* (Vol. 19, Issue 6). Springer Berlin Heidelberg.  
<https://doi.org/10.1007/s10237-020-01322-7>
30. Nikoghosyan, A. S., Shen, J., & Ting, H. (2019). Physical Properties of Human Jawbone, Spongy Bone, Collagen and Cerabone® Bone Transplantation Material in Range of 0.2 to 2.5 THz. *International Conference on Infrared, Millimeter, and Terahertz Waves, IRMMW-THz, 2019-Septe*, 1–2. <https://doi.org/10.1109/IRMMW-THz.2019.8873754>
31. O, A. L. (2006). *Dolor dorsolumbar inflamatorio con osteofitos marginales*. 97–100.
32. Ovadia, D. (2013). Classification of adolescent idiopathic scoliosis (AIS). *Journal of Children's Orthopaedics*, 7(1), 25–28. <https://doi.org/10.1007/s11832-012-0459-2>
33. Reilly, D. T., & Burstein, A. H. (1974). The mechanical properties of cortical bone. *Journal of Bone and Joint Surgery - Series A*, 56(5), 1001–1022.  
<https://doi.org/10.2106/00004623-197456050-00012>
34. Reis, P. B. P. S., Vila-Vicosa, D., Rocchia, W., & Machuqueiro, M. (2020). PypKA: A flexible python module for poisson-Boltzmann-based pKa calculations. *Journal of Chemical Information and Modeling*, 60(10), 4442–4448.

<https://doi.org/10.1021/acs.jcim.0c00718>

35. Richards, B. S., Sucato, D. J., Konigsberg, D. E., & Ouellet, J. A. (2003). Comparison of reliability between the Lenke and King classification systems for adolescent idiopathic scoliosis using radiographs that were not premeasured. *Spine*, 28(11), 1148–1156. <https://doi.org/10.1097/00007632-200306010-00012>
36. Rinella, A., Bridwell, K., Kim, Y., Rudzki, J., Edwards, C., Roh, M., Lenke, L., & Berra, A. (2004). Late Complications of Adult Idiopathic Scoliosis Primary Fusions to L4 and Above: The Effect of Age and Distal Fusion Level. *Spine*, 29(3), 318–325. <https://doi.org/10.1097/01.BRS.0000111838.98892.01>
37. Rittmeister, M., Leyendecker, K., Kurth, A., & Schmitt, E. (1999). Cauda equina compression due to a laminar hook: A late complication of posterior instrumentation in scoliosis surgery. *European Spine Journal*, 8(5), 417–420. <https://doi.org/10.1007/s005860050197>
38. Routh, R. H., Rumancik, S., Pathak, R. D., Burshell, A. L., & Nauman, E. A. (2005). The relationship between bone mineral density and biomechanics in patients with osteoporosis and scoliosis. *Osteoporosis International*, 16(12), 1857–1863. <https://doi.org/10.1007/s00198-005-1951-z>
39. Sun, X., Xie, Y., Kong, Q., Xu, X., Huan, L., Zhang, B., Sun, K., & Shi, J. (2018). Segmental Characteristics of Main Thoracic Curves in Patients with Severe Adolescent Idiopathic Scoliosis. *World Neurosurgery*, 119, e174–e179. <https://doi.org/10.1016/j.wneu.2018.07.086>
40. Shakil, H., Iqbal, Z. A., & Al-Ghadir, A. H. (2014). Scoliosis: Review of types of

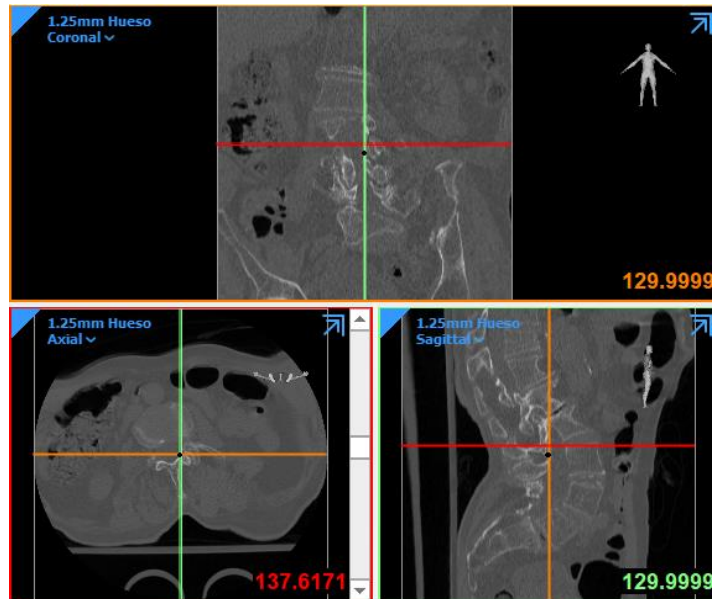
- curves, etiological theories and conservative treatment. *Journal of Back and Musculoskeletal Rehabilitation*, 27(2), 111–115. <https://doi.org/10.3233/BMR-130438>
41. Shao, Z., Rompe, G., & Schiltewolf, M. (2002). Radiographic changes in the lumbar intervertebral discs and lumbar vertebrae with age. *Spine*, 27(3), 263–268. <https://doi.org/10.1097/00007632-200202010-00013>
42. Taghi, M., Mohammad, K., Ebrahimi, H., & Mohammadi, A. (2016). Evaluation of the influences of various force magnitudes and configurations on scoliotic curve correction using finite element analysis. *Australasian Physical & Engineering Sciences in Medicine*, 0(0), 0. <https://doi.org/10.1007/s13246-016-0501-7>
43. Upct, M. (2013). *Guía docente de la asignatura Métodos numéricos para la modelización Guía Docente*. 2012–2013.
44. Kardong, Kenneth V., cop. (2007). *Vertebrados anatomía comparada, función, evolución*, por, 4a ed edición, McGraw-Hill / Interamericana de España.
45. Vialle, R., Thévenin-Lemoine, C., & Mary, P. (2013). Neuromuscular scoliosis. *Orthopaedics and Traumatology: Surgery and Research*, 99(1), S124–S139. <https://doi.org/10.1016/j.otsr.2012.11.002>
46. *Vim online*. (s/f). Vim.org. Recuperado el 12 de septiembre de 2021, de <https://www.vim.org/>
47. Wang, W., Baran, G. R., Betz, R. R., Samdani, A. F., Pahys, J. M., & Cahill, P. J. (2014). The Use of finite element models to assist understanding and treatment for scoliosis: A review paper. *Spine Deformity*, 2(1), 10–27.

<https://doi.org/10.1016/j.jspd.2013.09.007>

48. Wikipedia contributors. (s/f). ANSYS. Wikipedia, The Free Encyclopedia. Recuperado el 12 de septiembre de 2021, de <https://es.wikipedia.org/w/index.php?title=ANSYS&oldid=135608150>
49. Yuing, F. T. A., Almagià, A. F., Lizana, P. J., Rodríguez, R. F. J., Ivanovic, D. M., Binvignat, G. O., Gallardo, L. R., Nieto, C. F., & Verdejo, S. A. (2010). Comparación entre Dos Métodos Utilizados para Medir la Curva Lumbar. *International Journal of Morphology*, 28(2), 509–513. <https://doi.org/10.4067/s0717-95022010000200028>

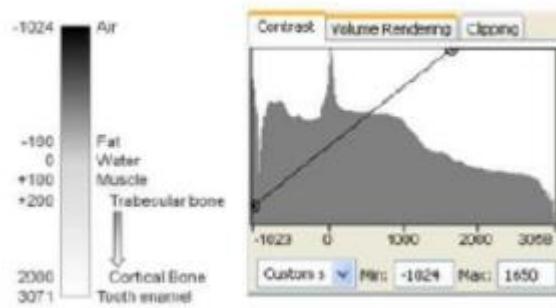
### 13. Anexos

- Different CT views in mimics materialize software

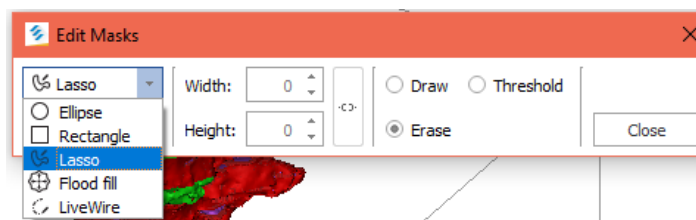


Annex 1. Coronal, axial ,and sagittal views of a CT scan

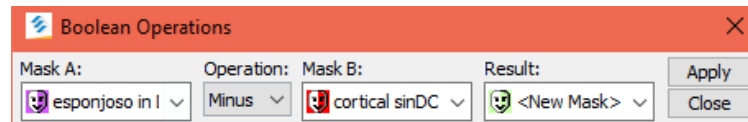
- Design modeling in Mimics Materialise



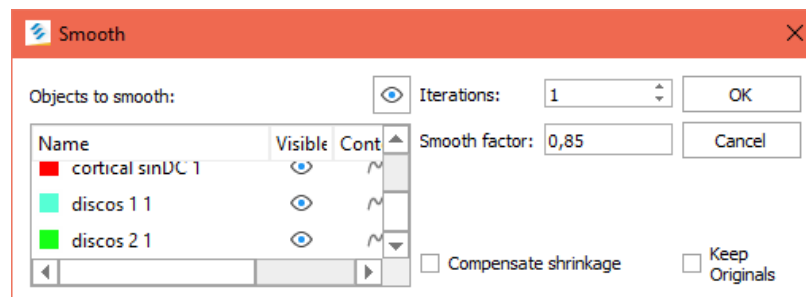
Annex 2. Contrast interface



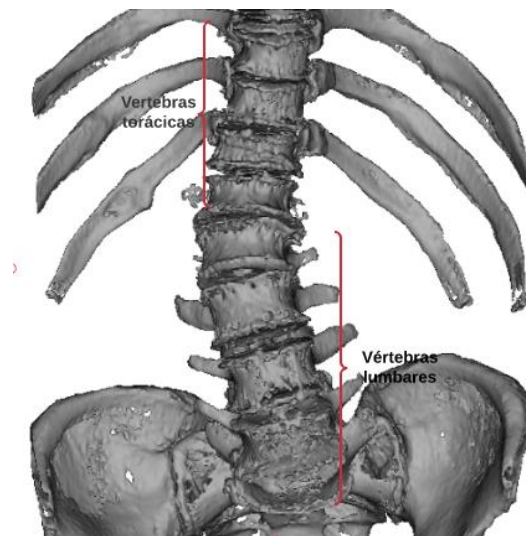
*Annex 3.* interface to edit mask, use of lasso tool to select the area.



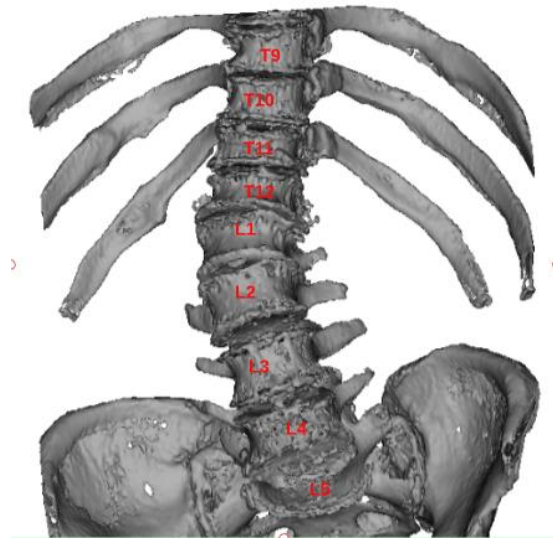
*Annex 4.* interface for Boolean operation used to add or subtract mask



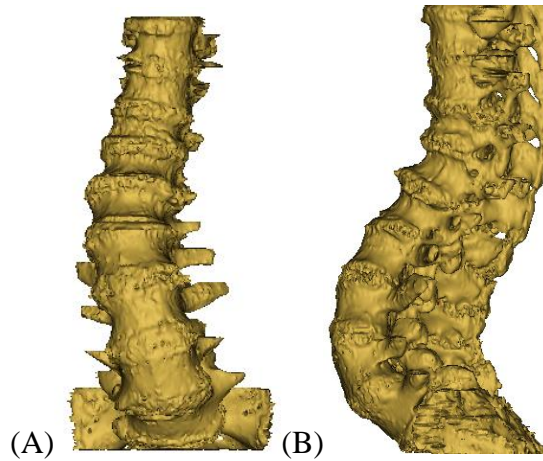
*Annex 5.* interface to smooth the 3D model



*Annex 6.* Coronal view of the end of the dorsal vertebrae, lumbar-sacral vertebrae coccyx, floating ribs, and hip.

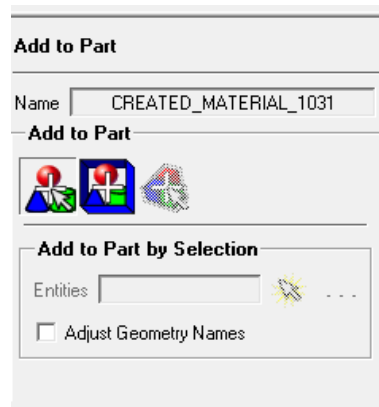


*Annex 7.* Arrangement of each vertebra in the coronal plane



*Annex 8.* (A) Coronal view of the final vertebrae of the dorsal and lumbar region. (B) Sagittal view of the final vertebrae of the dorsal and lumbar region.

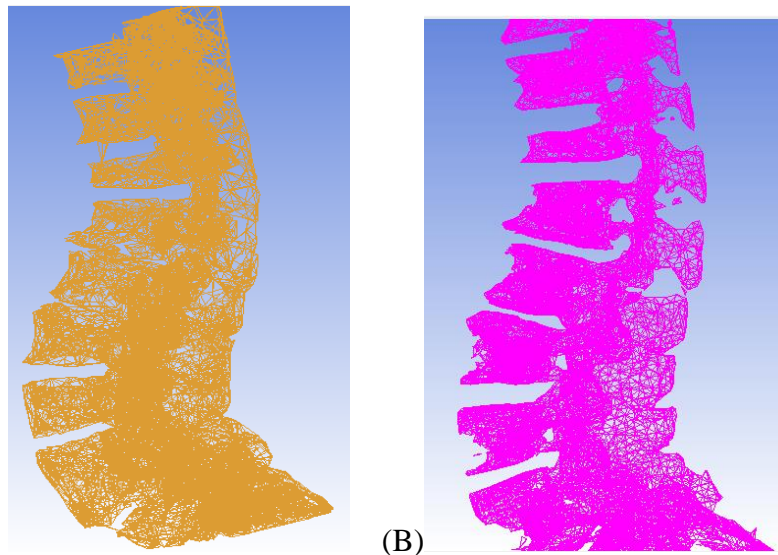
- Meshing the design in Ansys (Icem)



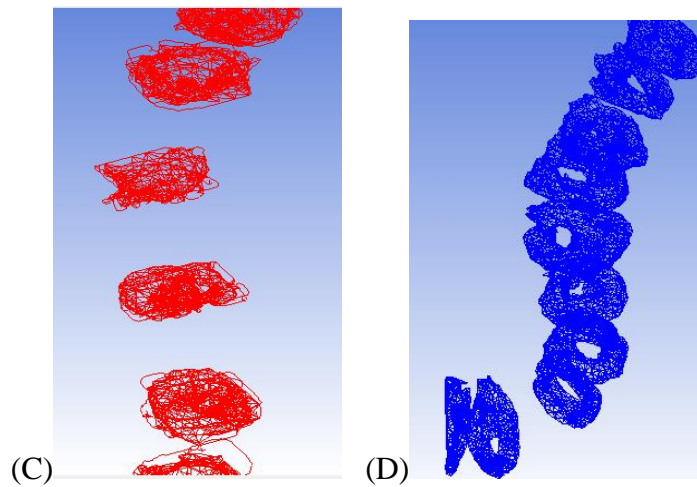
*Annex 9.* Add to part tool interface.



*Annex 10.* General meshing of the model, ribs, vertebrae, hips.



*Annex 11.* Mesh of the model. (A) section of the cortical bone area, (B) section of the cancellous bone area.



*Annex 12.* Mesh of the model. (C) section of the core area of the vertebral (D) section of the area of the annulus matrix vertebra.

- Data for Finite element model of FSU

Components of FSU	Young's mod. (Mpa)	Poisson's ratio
Vertebral cortical bone	12000	0.3
Vertebral cancellous bone	150	0.3

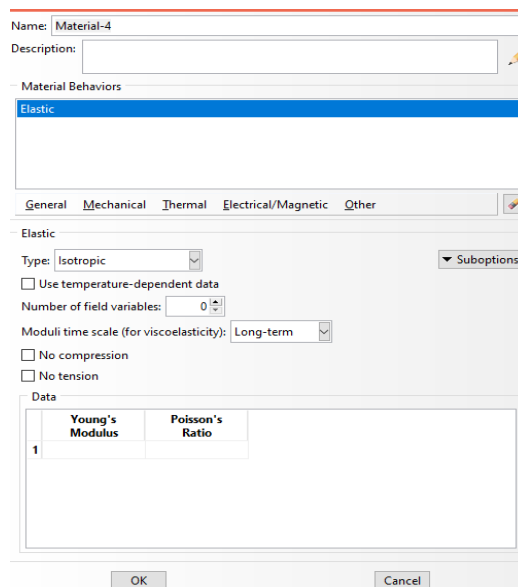
*Annex 13.* Material moduli of the components of FSU; adapted from, Kurutz, M., & Oroszváry, L. (2010). Finite element analysis of weightbath hydrotraction treatment of

degenerated lumbar spine segments in elastic phase. Journal of Biomechanics, 43 (3), 433–441. doi: 10.1016 / j.jbiomech.2009.10.004

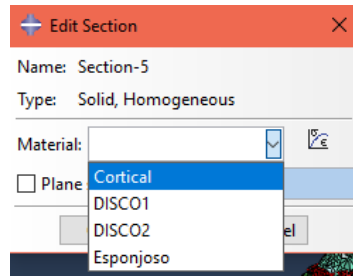
Modeling the degeneration of aging: material moduli from healthy (1) to fully degenerated (5) components of FSU.

Grades of age-related degeneration	1 (healthy)	2	3	4	5 (fully deg.)
<b>For compression</b>					
<b>Nucleus</b>					
Young's modulus	1	3	9	27	81
Poisson's ratio	0.499	0.45	0.4	0.35	0.3
<b>Annulus matrix</b>					
Young's modulus	4	4.5	5	5.5	6
Poisson's ratio	0.45	0.45	0.45	0.45	0.45

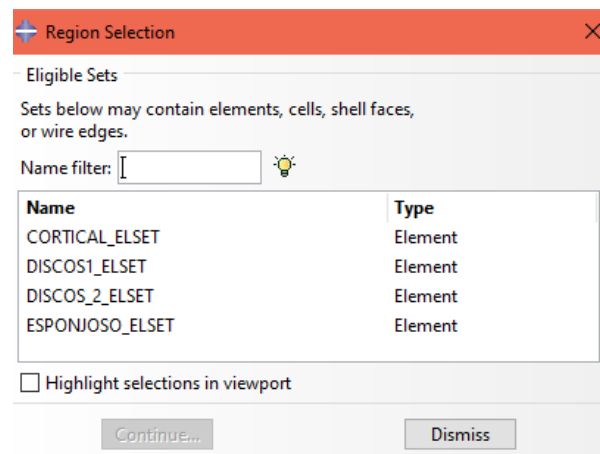
*Annex 14.* Modeling the degeneration of aging: material moduli from healthy (1) to fully degenerated (5) components of FSU; adapted from Kurutz, M., & Oroszváry, L. (2010). Finite element analysis of weightbath hydrotraction treatment of degenerated lumbar spine segments in elastic phase. Journal of Biomechanics, 43 (3), 433–441. doi: 10.1016 / j.jbiomech.2009.10.004



*Annex 15.* Material creation interface in Abaqus.



*Annex 16.* Abaqus selection creation interface.



*Annex 17.* Abaqus assignment selection creation interface.

- Abaqus interpolation in Gvim

```

** *****
*Heading
** Job name: simulacion3-copy2 Model name: cambio-Copy2
** Generated by: Abaqus/CAE 2020
**Preprint, echo=NO, model=NO, history=NO, contact=NO
**
** PARTS
**
*Part, name=PART-1
*Node
+--65007 lines: 1, -3.60395527, 52.9120598, 43.5305901-----
*Element, type=C3D4
+--276365 lines: 128685, 11621, 23284, 50239, 13845-----
*Elset, elset=CORTICAL_ELSET
+--8843 lines: 128685, 128687, 128690, 128691, 128693, 128694, 128695, 128699, 128700, 128703, 128704, 128705, 128709, 128712, 128713, 128715-----
*Elset, elset=DISCOS_ELSET
+--2313 lines: 128686, 128688, 128689, 128697, 128706, 128707, 128740, 128752, 128777, 128784, 128787, 128791, 128792, 128797, 128798, 128808-----
*Elset, elset=ESPONJOSO_ELSET
+--6119 lines: 128692, 128696, 128698, 128701, 128702, 128708, 128710, 128711, 128714, 128721, 128730, 128732, 128733, 128734, 128735, 128741-----
** Section: Section-C
*Solid Section, elset=CORTICAL_ELSET, material=Material-C
,
** Section: Section-D
*Solid Section, elset=DISCOS_ELSET, material=Material-C
,
** Section: Section-E
*Solid Section, elset=ESPONJOSO_ELSET, material=Material-E
,
*End Part
**
**
** ASSEMBLY
**
*Assembly, name=Assembly
**
*Instance, name=PART-1-1, part=PART-1
*End Instance
**
**
*Nset, nset=ALL, instance=PART-1-1
+--4063 lines: 1, 2, 3, 4, 5, 6, 7, 8, 9, 10, 12, 13, 15, 17, 19, 20-----
*Elset, elset=CORTICAL_ELSET, instance=PART-1-1
+--8843 lines: 128685, 128687, 128690, 128691, 128693, 128694, 128695, 128699, 128700, 128703, 128704, 128705, 128709, 128712, 128713, 128715-----
*Nset, nset=CORTICAL_NSET, instance=PART-1-1
+--2990 lines: 1, 2, 3, 4, 5, 6, 8, 9, 10, 12, 13, 15, 17, 19, 21, 22-----
*Elset, elset=DISCOS_ELSET, instance=PART-1-1
+--2313 lines: 128686, 128688, 128689, 128697, 128706, 128707, 128740, 128752, 128777, 128784, 128787, 128791, 128792, 128797, 128798, 128808-----
*Nset, nset=DISCOS_NSET, instance=PART-1-1
+--818 lines: 4, 7, 12, 26, 48, 54, 55, 56, 57, 58, 72, 79, 86, 95, 101, 104-----
*Elset, elset=ESPONJOSO_ELSET, instance=PART-1-1
+--6119 lines: 128692, 128696, 128698, 128701, 128702, 128708, 128710, 128711, 128714, 128721, 128730, 128732, 128733, 128734, 128735, 128741-----
*Nset, nset=ESPONJOSO_NSET, instance=PART-1-1
+--2533 lines: 1, 2, 3, 4, 5, 6, 7, 8, 9, 10, 12, 13, 15, 19, 20, 21-----
*Nset, nset=Set-9, instance=PART-1-1
+--110 lines: 4, 49, 50, 51, 224, 264, 345, 358, 381, 382, 393, 454, 623, 678, 679, 848-----
*Nset, nset=base, instance=PART-1-1
+--196 lines: 10, 42, 53, 72, 103, 106, 193, 194, 197, 230, 231, 232, 259, 260, 360, 383-----
*Elset, elset=Surf-1_S1, internal, instance=PART-1-1
+-- 31 lines: 136700, 137272, 138229, 139446, 139944, 140302, 140786, 141823, 142056, 142159, 143399, 143639, 143971, 144645, 145830, 148995-----
*Elset, elset=Surf-1_S2, internal, instance=PART-1-1
+-- 33 lines: 130855, 130916, 131795, 136075, 136699, 136860, 136905, 138820, 138822, 142889, 143972, 144891, 147426, 151120, 151145, 151152-----
*Elset, elset=Surf-1_S3, internal, instance=PART-1-1
+-- 63 lines: 129078, 129090, 129091, 129401, 130668, 131026, 131081, 131249, 131263, 131625, 131662, 131898, 132199, 132447, 132739, 132997-----
*Elset, elset=Surf-1_S4, internal, instance=PART-1-1
+-- 57 lines: 129090, 129091, 129368, 130614, 130615, 130825, 130928, 131163, 131383, 131431, 131545, 131652, 131737, 131898, 131935, 131936-----
*Surface, type=ELEMENT, name=Surf-1
+-- 4 lines: Surf-1_S1, S1-----
*Elset, elset=Surf-2_S1, internal, instance=PART-1-1
+-- 83 lines: 128809, 131565, 131770, 132732, 134553, 135316, 135336, 135786, 136320, 136506, 137676, 137894, 138546, 139296, 139310, 139885-----
*Elset, elset=Surf-2_S2, internal, instance=PART-1-1
+-- 78 lines: 129458, 131159, 131217, 131942, 133855, 134242, 134243, 134271, 134828, 136219, 136319, 136393, 136504, 136943, 137221, 137277-----
*Elset, elset=Surf-2_S3, internal, instance=PART-1-1
+--157 lines: 128991, 129337, 129516, 130164, 130167, 130170, 130171, 130442, 130833, 131023, 131194, 131195, 131217, 131298, 131314, 131403-----
*Elset, elset=Surf-2_S4, internal, instance=PART-1-1
+--147 lines: 128748, 128886, 128923, 128990, 129082, 129113, 129129, 129146, 129449, 129713, 129772, 130094, 130168, 130170, 130618, 130648-----
*Surface, type=ELEMENT, name=Surf-2

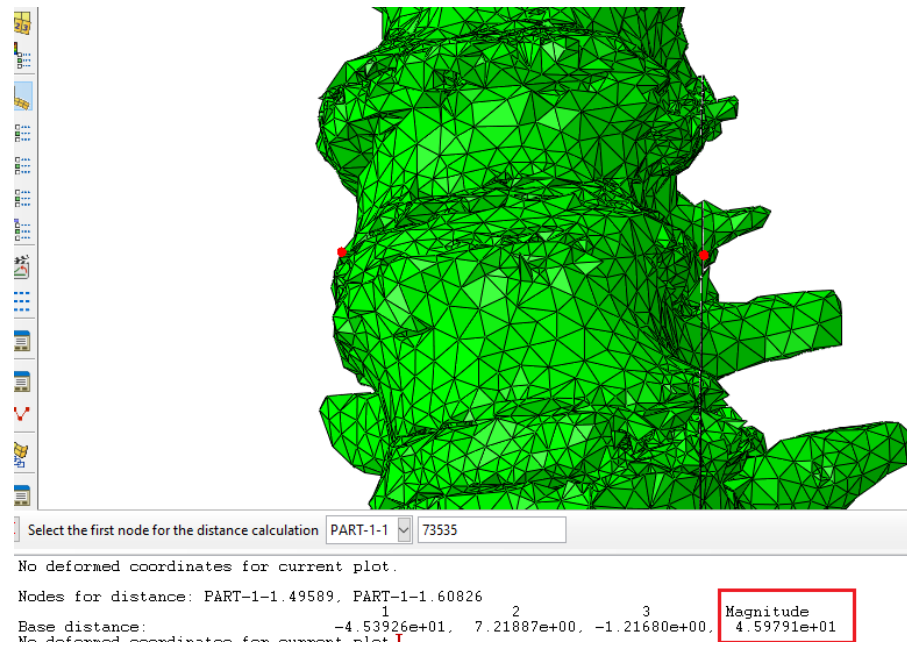
```

```

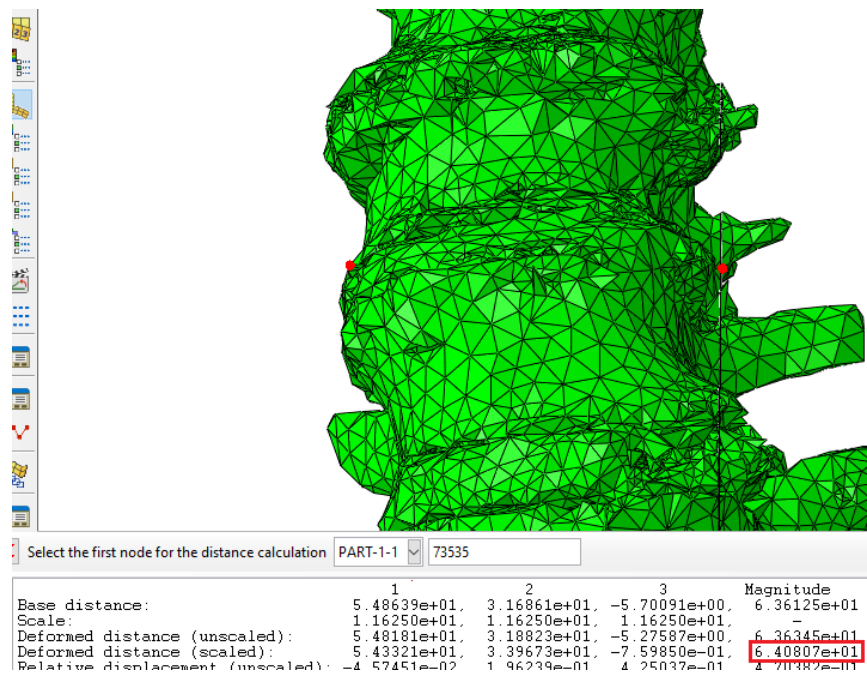
*End Assembly
**
** MATERIALS
**
*Material, name=Material-C
*Elastic
1200., 0.3
*Material, name=Material-D
*Elastic
9., 0.4
*Material, name=Material-E
*Elastic
150., 0.3
**
** BOUNDARY CONDITIONS
**
** Name: Base Type: Symmetry/Antisymmetry/Encastre
*Boundary
base, ENCASTRE
-----
**
** STEP: Step
**
*Step, name=Step, nlgeom=NO, inc=1000
*Static, stabilize, allsdtol=0.05, continue=YES
1., 100., 1e-05, 1.
**
** LOADS
**
** Name: Load-1 Type: Pressure
*Dsload
Surf-1, P, 0.43
**
** OUTPUT REQUESTS
**
*Restart, write, frequency=0
**
** FIELD OUTPUT: F-Output-1
**
** *Output, field, variable=PRESELECT
**
** HISTORY OUTPUT: H-Output-1
**
** *Output, history, variable=PRESELECT
** *End Step
~

```

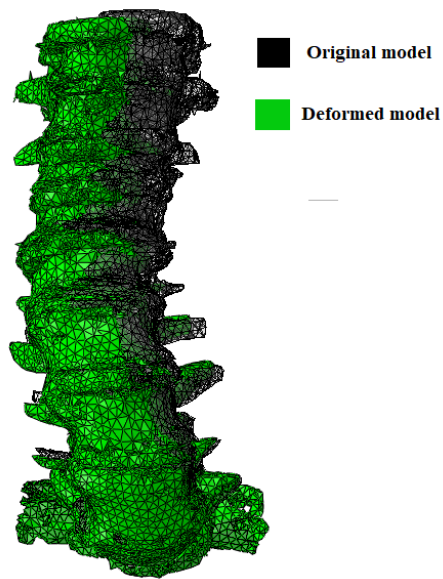
*Annex 18.* Gvim code generation of the simulation.



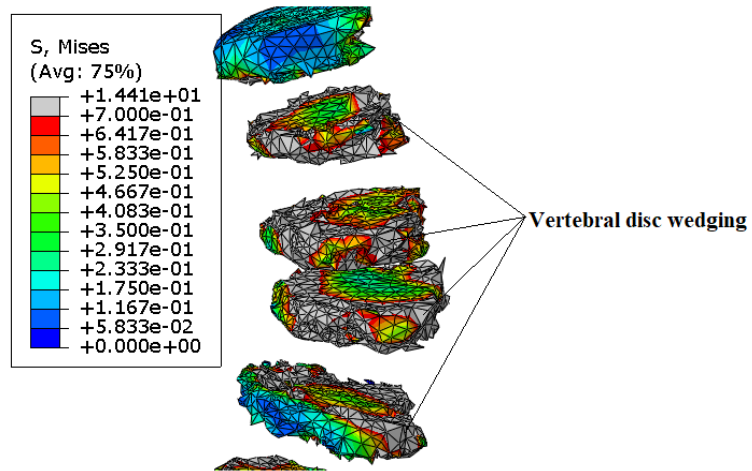
Annex 19. Distance between the x-plane and the greatest curvature of the original model.



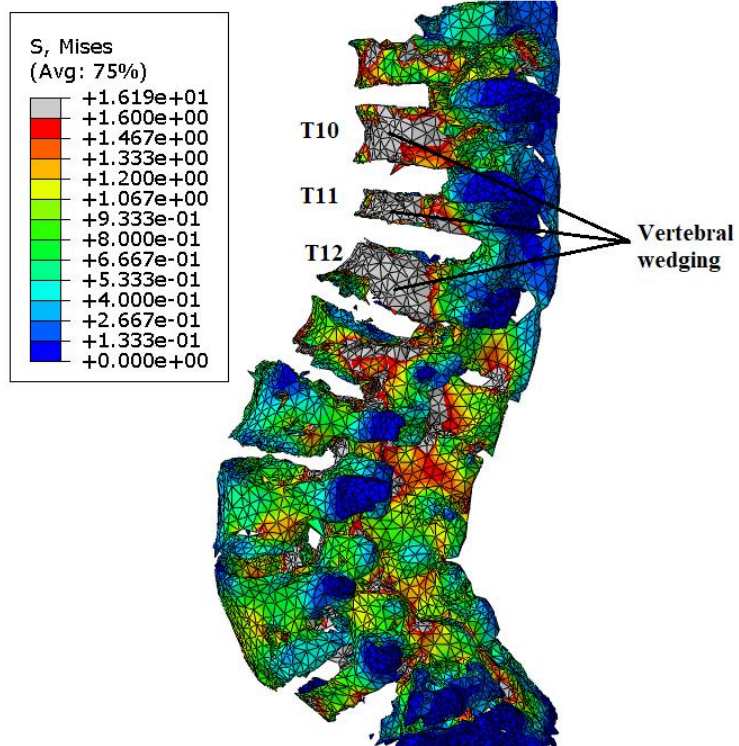
Annex 20. Distance between the x-plane and the greatest curvature of the deformed model.



Annex 21. Correlation between the original model and the deformed one.



Annex 22. Zones of Vertebral disc wedging (white part)



Annex 23. Zones of Vertebral wedging (white part)